RESEARCH ARTICLE

Key Points:
- This study presents for the first time a comprehensive analysis of the average CEJ characteristics based on CHAMP satellite observations
- The CEJ dependencies on local time, season, geomagnetic activity, and solar activity are investigated
- The influences of solar and lunar tides on CEJ occurrences and the CEJ response to sudden changes of solar wind input are presented

Comprehensive Analysis of the Counter Equatorial Electrojet: Average Properties as Deduced From CHAMP Observations

Yun-Liang Zhou[1] (iD)**, Hermann Lühr[2], Hong-wen Xu[1], and Patrick Alken[3]** (iD)

[1]Department of Space Physics, School of Electronic Information, Wuhan University, Wuhan, China, [2]GFZ, German Research Centre for Geosciences, Section 2.3, Geomagnetism, Potsdam, Germany, [3]Cooperative Institute for Research in Environmental Sciences, University of Colorado, Boulder, CO, USA

Abstract Ten years of geomagnetic field observations by the CHAMP satellite are used for a systematic investigation of the counter equatorial electrojet (CEJ). For the first time a comprehensive characterization of CEJ is presented. CEJs occur preferably during early morning, and their occurrence rate is down to 4% at noon. The CEJ occurrence rate shows a clear annual variation with a peak around July–August and a secondary peak in January. The late summer peak is related to the effect of meteor dust ablation. The CEJ amplitude is closely controlled by magnetic activity, showing a good correlation with the a_P index. Nonmigrating solar tides are the main reason for longitudinal patterns of occurrence rate. The most prominent wavenumber 1 longitudinal structures during all seasons can be attributed to the tidal components SW3 and SPW1. The wavenumber 4 becomes largest during late summer-autumn season, which is related to the DE3 component. Also, the influence of lunar tides is evident in the CEJ occurrence rate. Strongest modulation of the CEJ by the semidiurnal lunar M2 tide is observed around January, which is responsible for the secondary CEJ occurrence peak in January. Both the solar and lunar tidal waves appear out of phase between CEJ and equatorial electrojet, implying that the same tidal mechanisms influence both current systems. Changes of solar wind conditions can also influence the CEJ. Immediately after a sudden increase of solar wind input CEJs are depressed, but about 3 hr after that event CEJs are strongly enhanced because of the disturbance wind dynamo.

1. Introduction

The equatorial electrojet (EEJ) is a confined electric current flowing within a narrow latitudinal band along the magnetic equator in the ionosphere *E* region. Usually the direction of this current is eastward during daytime. However, the typical eastward electric current is sometimes reversed, which was first inferred by Gouin (1962) from the negative deflection of the horizontal magnetic field around local noon at Addis Ababa, Ethiopia. This narrow band of the reversed current is termed the counter equatorial electrojet (CEJ), as first proposed by Gouin and Mayaud (1967).

Since its discovery the characteristics of CEJ and its dependences on local time, season, longitude, moon phase, geomagnetic activity, and solar activity have been the topic of numerous studies based on ground-based and satellite magnetic data for several decades (e.g., Marriot et al., 1979; Mayaud, 1977; Onwumechili, 1997; Rastogi, 1974a; Vichare & Rajaram, 2011). By using the magnetic field observations from equatorial stations Davao (Philippines), Kodaikanal (India), Addis Ababa (Ethiopia), Freetown (Sierra Leone), and Huancayo (Peru), the local time variation of the occurrence of the daytime depressions in the geomagnetic horizontal component, which is related to the CEJ, are investigated by Rastogi (1974a). It is reported that the CEJ events are generally observed around morning (0700 LT) and evening (1600 LT), and from the yearly averaged data the number of CEJ events during evening hours are larger than that of the morning events. By utilizing magnetic measurements from Magsat, a spacecraft in dawn-dusk orbit, Cohen and Achache (1990) suggested that the CEJ effect was measured around dawn most of the time. Based on 1-year magnetic data from the Ørsted satellite, the local time variation of the CEJ occurrence was also analyzed by Vichare and Rajaram (2011). They reported that the peak in CEJ occurrence rate around 1200–1300 LT is larger than the peak around 0800–1000 LT. Due to the limited span of data, they could not provide the CEJ occurrence for all daytime hours. It seems that the local time dependence of the CEJ occurrence is not yet very clear.

The CEJ occurrence frequency obviously exhibits a prominent seasonal dependence. Early in 1970 it was reported that the afternoon CEJ shows a clear maximum at Zaria, Nigeria, for the December solstice

(Hutton & Oyinloye, 1970). Based on the observations from the stations in four different longitude sectors, South American (Huancayo), African (Freetown and Addis Ababa), Asian (Kodaikanal) and the Pacific (Koror) sectors, some publications stated that the morning CEJ events are generally more frequent during the equinoxes than during the winter or summer months, and the evening events are more frequent during summer than during winter months (Marriot et al., 1973, 1979; Mayaud, 1977). On the other hand, Vichare and Rajaram (2011) reported that the CEJ occurrence frequency maximizes during the months June–August and a secondary peak occurs in January. They found no single CEJ event in the months of February, October, and November. For the seasonal variation of the CEJ there are obviously some contradicting results published.

Regarding the solar cycle variation of the CEJ, some discrepancies can also be found in previous publications. Gouin and Mayaud (1967) reported larger amplitudes of the morning negative depression in the horizontal magnetic field deflection at solar maximum from ground-based data at Addis Ababa, Ethiopia. However, Hutton and Oyinloye (1970) obtained at Zaria, Nigeria, in general a larger number of CEJ events at solar minimum. By comparing the number of sunspots with the occurrence of the CEJ events, Marriot et al. (1973, 1979) reported that the afternoon CEJ events at Huancayo, Peru, are much more frequent during solar minimum. In contrast to the afternoon CEJ events, the morning CEJ events at Huancayo do not show clear correlation with the number of the sunspot. It seems there is so far no paper, based on satellite observation, to investigate the variation of the CEJ with the solar activity.

The longitudinal variation of the CEJ occurrence is also a topic of many studies. Shortly after the discovery of the CEJ event, based on the measurements from the magnetograms at Trivandrum and Annamalainagra, India, Rao and Rajarao (1963) indicated that CEJ events are absent during the same days as examined by Gouin (1962) at Addis Ababa. By comparing the variation of the geomagnetic horizontal component from the station Addis Ababa (Ethiopia) and Kodaikanal (India), Rastogi (1973) reported that the depression in the horizontal geomagnetic component is different at different equatorial stations. He concluded that the afternoon depression in the horizontal component is localized in longitude, and sometimes the CEJ events may not appear on the same day even at locations separated by only 30° in longitude. However, Mayaud (1977) considered for a given event that CEJ would not seem to occur in a very narrow longitude (2 or 3 hr). In a statistical study based on magnetic measurements from CHAMP McCreadie (2004) found that the CEJ occurrence rate shows a longitudinal variation with peaks at longitudes near 60°, 165°, 255°, and 335°. However, by considering a data period of only little more than 2 years, a beating between seasonal and local time variations biases the results. By using the Ørsted satellite data, Vichare and Rajaram (2011) reported that the longitudinal extent of the CEJ phenomenon is often restricted to less than 25° in longitude. They also found that the CEJ occurrence is maximum in the longitudinal region from 300° to 330°E. And the secondary peak of CEJ occurrence rate lies in the region of 150°–240°E. Recently, Chandrasekhar et al. (2017) characterized the variability of CEJ at a longitudinal separation of about 15° by using hourly averaged variation at two EEJ pairs of stations (Hyderabad and Vencode at 77°E and Port Blair and Campbell Bay at 93°E). They found that the occurrence of CEJ is not simultaneous for about 40% of the events at the two longitudes.

Additionally, the occurrence rate of CEJ seems to show an important modulation by the moon phase. Based on ground observations of the geomagnetic field at Huancayo (Peru) from 1948 to 1971, Rastogi (1974b) reported that the occurrence of evening (1500–1700 LT) CEJ events maximizes around lunar times 2.2 and 14.2 hr, and morning (0700 LT) events around 4.8 and 16.8 hr. He pointed out that these lunar times correspond to the minima in horizontal component, attributed to the modulation by the lunar tidal wave. By using the geomagnetic data at Trivandrum, India, during the period 1959–1978, Sastri and Arora (1981) indicated that a large lunar modulation on the CEJ occurrence is observed in January. They attributed this phenomenon to the global enhancement of the lunar tide during January. Stening (2011) also reported that the afternoon CEJ events are frequent at new moon and full moon during stratospheric sudden warming events.

Besides the characteristics of the CEJ events, the mechanisms causing the CEJ phenomenon have drawn great attention for several decades. Many possible mechanisms have been proposed for the interpretation of the CEJ events. First, the neutral wind is often used to explain CEJ. By using the observations of mean winds and the amplitude and phases of the tidal components at Trivandrum (India), Somayajulu et al. (1993) found that the zonal wind is predominately westward (eastward) at the height of 90–105 km during days with (without) CEJ events. The amplitudes and phases of the tidal components on the days with CEJ events are different from those days without CEJ events. Raghavarao and Anandarao (1980) indicated that vertical winds can be a

plausible cause for the CEJ. Second, the CEJ is also thought to be related to the reduction in the daytime mesopause temperature in connection with atmospheric gravity waves of lower atmospheric origin (Vineeth et al., 2012). In addition to the aforementioned plausible cause, the lunar tides take an important role in the production of CEJ events (Rastogi, 1974b; Sastri & Arora, 1981; Stening, 2011). It was suggested by Stening (2011) that there is an amplification of lunar tides during times of stratospheric sudden warmings around January when the CEJ occurrence frequency is high. Additionally, Chen et al. (1995) suggested that the quasi-biennial oscillation is a possible mechanism for favoring the CEJ. Vineeth et al. (2016) indicated that the presence of meteor showers can play an important role for the generation of the CEJ. They showed that a strong dust layer produced by meteoric ablation in the lower E region can lead to a significant modification of the vertical polarization electric field. Such a dust layer gets negatively charged by attracting the electrons, thus causing a polarization electric field in the downward direction and leading to another current in westward direction in the bottomside E region. If this current is strong enough, it can lead to a reversal of the EEJ signature. Furthermore, the solar wind input is another possible source of CEJ. Kikuchi et al. (2000) suggested that a northward turning of the interplanetary magnetic field (IMF) caused a westward pointing prompt penetrating electric field that favors the CEJ. Finally, the westward electric field setup a few hours after the start of magnetic activity by the disturbance wind dynamo can cause the generation of CEJ.

In summary, there are obviously many effects that can cause the CEJ. Although it has been studied extensively for several decades, there is no consensus on the relative importance of the various effects causing the reversal of EEJ current flow. It would require a comprehensive climatology of the CEJ occurrences in order to separate the relative influences of the different drivers. By utilizing 10 years of high-accuracy CHAMP magnetic field measurements, we present an unprecedented detailed analysis revisiting the CEJ characteristics and its dependences on local time, seasons, longitude, solar tides, moon phase, and the geomagnetic and solar activity. We also address the CEJ response to sudden changes of solar wind input. The large number of electrojet crossings (more than 52,000) allows for an unbiased and dedicated investigation of all these various dependences.

In section 2 we will describe the data set and the processing approach. The observational results will be presented in section 3. Then we will discuss our observational results in the context of previous studies. The main findings are summarized in section 5.

2. Data

The basis for our CEJ study are the magnetic field data sampled every second by the absolute Overhauser Magnetometer onboard the CHAMP satellite (Reigber et al., 2002). The CHAMP was launched in July 2000 into a circular, near-polar orbit at 450 km altitude. After more than 10 years of operation its altitude had decayed to 250 km and the spacecraft reentered the atmosphere in September 2010.

2.1. Deducing EEJ Profiles From Magnetic Field Data

Conventionally the EEJ characteristics have been directly derived from the magnetic field distribution on ground under the magnetic equator. This approach is not so suitable for satellites because of the varying orbital altitude above the E region. We rather used the more general current density latitudinal profiles as basis for this study. The technique employed for inverting the scalar magnetic field recordings along the orbit in terms of a series of line currents at E region altitude was first described by Lühr et al. (2004) and later refined by Alken et al. (2013, 2015). In this study we follow the same approach as described in Zhou et al. (2018). Here we list just the main processing steps. First the core, crustal, and magnetospheric field contributions are removed from the original field readings. For these purposes we make use of the CHAOS-6, MF7, and POMME-6 models for subtracting the respective field parts. The contributions of mid-latitude Sq currents and unmodeled external fields are filtered out on a track-by-track basis. Finally, the diamagnetic effect caused by pressure gradient of the ambient plasma is eliminated. The residual magnetic field variations are assumed to represent the clean EEJ signal. This is the basis for the field inversion to derive latitude profiles of the height-integrated sheet current density in the vicinity of the equator. For a more detailed description of the EEJ profile derivation the reader is referred to Alken et al. (2013, 2015, and references therein).
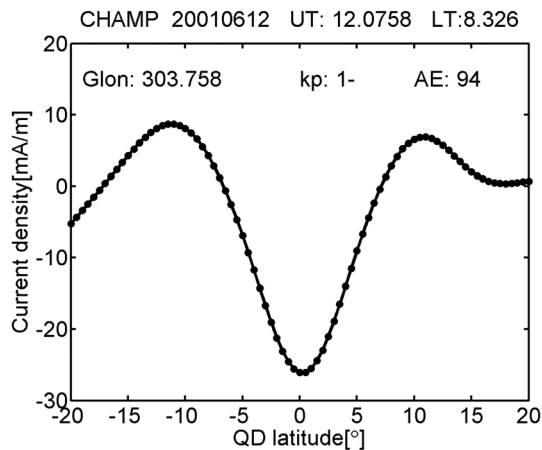
Figure 1. Example of a typical profile of counter equatorial electrojet height-integrated current density derived by inverting CHAMP magnetic field measurements.

2.2. CEJ Events Selection

Based on the latitudinal profiles of the electrojet current density derived by the aforementioned approach, we select the CEJ events occurring during the time from August 2000 to February 2010, spanning nearly a solar cycle. Within this period the CHAMP satellite has crossed the dayside equator over 52,200 times in total, providing an even coverage of local times during all seasons. For these equator crossings the CEJ events are picked out by a rigorous selection procedure. First, we select events that show significant westward currents near the magnetic equator. Second, the peak amplitude of the westward current density has to exceed 10 mA/m, and the peak current density has to appear within $\pm 1°$ quasi-dipole (QD) latitude. Only those events are considered in the statistical analysis of this study. By taking these three conditions into account, 7,258 clear CEJ events are selected. The proportion of these CEJ events out of all reliable 40,160 electrojet profiles amounts to about 18%. Here the considered reliable electrojet profiles denote the EEJ (CEJ) events for which the peak amplitude of current density is larger than 10 mA/m, and the peaks occur within $\pm 1°$ QD latitude.

Figure 1 presents a typical example of the current density latitudinal profile of CEJ that occurred on 12 June 2001 shortly after 12 UT over South America (303.8° longitude). The graph depicts some general features of a morning (8.3 LT) CEJ event. At this time quiet geomagnetic activity prevailed ($Kp = 1^-$ and $AE = 94$). Clearly visible in the graph is the westward (negative) current peaking at the magnetic equator reaching a density of -26 mA/m. Off the magnetic equator, exceeding 7° in latitude, the current reverses from westward to eastward, showing eastward peak current densities around $\pm 11°$ QD latitudes. The amplitudes of these eastward peak current densities are 8.7 and 6.9 mA/m in the Southern and Northern Hemispheres, respectively. In this study we do not consider any further these reverse current sidebands. Beyond $\pm 15°$ QD latitude the current densities in both hemispheres become small. For the event presented here we observe a half-maximum width (HMW) of about 8° in latitude.

Figure 2 shows the distribution of occurrence rates for the different CEJ peak amplitudes. Here 100% represents the total number of 7,258 CEJ events. Amplitudes around 20 mA/m are most commonly observed. About 70% of all cases have amplitudes less than 35 mA/m. For larger CEJ events the rate decays rapidly, but there are also some cases with peak amplitudes exceeding 160 mA/m. The global average peak amplitude of all our CEJ events is 25 mA/m.
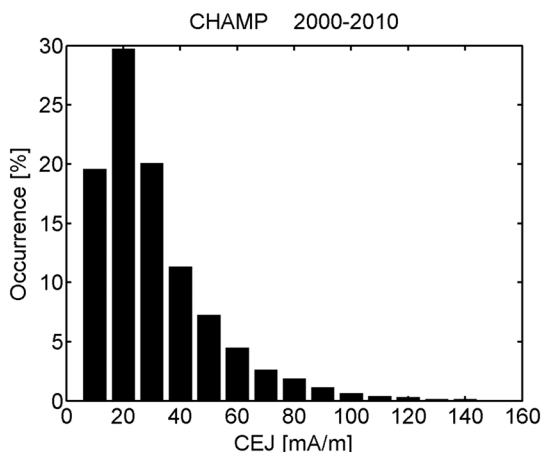
3. Observations

By using the selected CEJ events during 2000–2010, we first analyze the dependences of the amplitude and occurrence frequency on local time, season, longitude, geomagnetic activity, solar activity, and the moon phase. In sections 3.3 and 3.4 influences of the solar and lunar tides on CEJ occurrence rates are presented, respectively. Finally, we investigate the response of the CEJ to sudden changes on solar wind input.

3.1. Average Characteristics of the CEJ Amplitude

Figure 3 presents the peak amplitude variation of the CEJ with respect to several parameters including local time, season, longitude, Kp index, solar radio flux, and moon phase. For investigating the characteristics of the CEJ amplitude, we first search for the peak current density of each selected CEJ events, which is taken as the CEJ amplitude. And then the amplitudes are sorted into bins of the aforementioned quantity. Finally, the mean value of the CEJ amplitudes within each bin is plotted as a dot. For each mean value its uncertainty is plotted as black vertical bar. Here the uncertainty is defined as $\sigma/\sqrt{n}$, where σ and n are the standard deviation and the number of events in each bin, respectively.

Figure 2. Occurrence distribution of CEJ peak current density amplitudes. CEJ = counter equatorial electrojet.
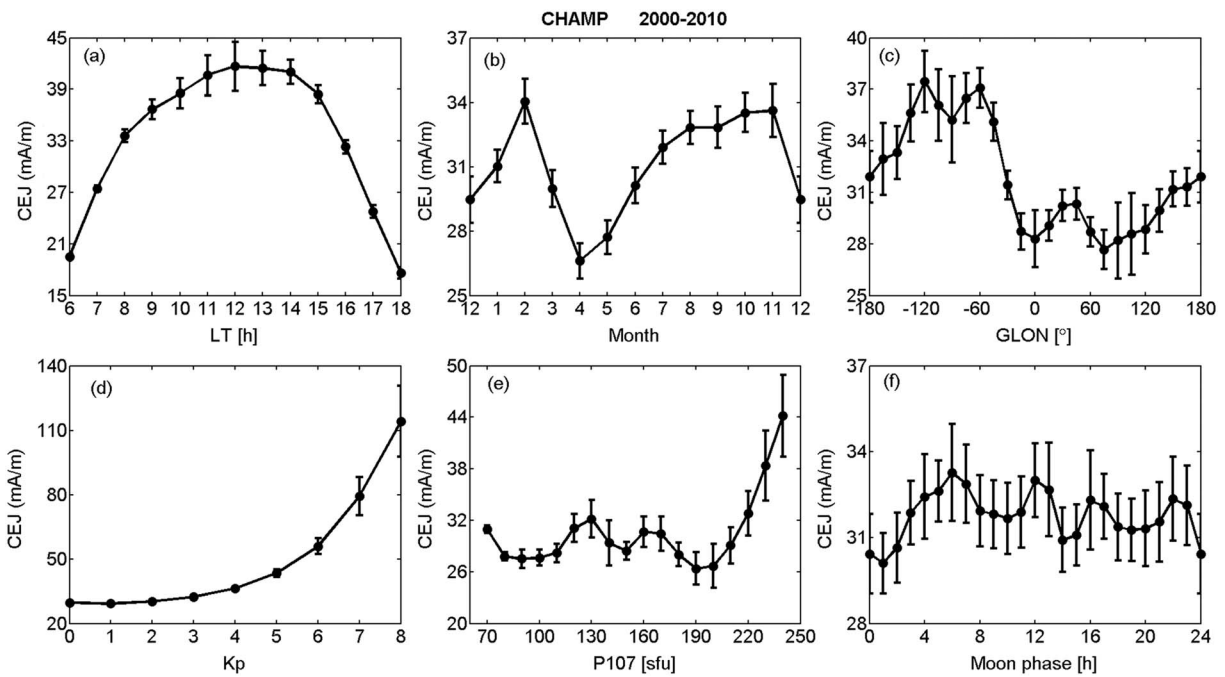
Figure 3. Dependence of CEJ amplitude on (a) local time (LT), (b) season, (c) longitude, (d) *Kp* index, (e) solar flux index (*P10.7*), and (f) moon phase. The black bars denote the uncertainties of the mean values. Too small bars are not visible here and in later figures. CEJ = counter equatorial electrojet.

Figure 3a provides the amplitude variation over local time from 0600 to 1800 LT. It can be seen that the CEJ amplitude exhibits a clear diurnal variation. The maximum amplitude is found at noontime with an average value of almost 41 mA/m. Toward morning and evening hours the amplitudes of the CEJ become smaller, approaching current densities less than 20 mA/m.

Figure 3b shows the seasonal variation. Mean values of the CEJ amplitude are plotted for each month of the year. One can see that the CEJ reaches larger amplitudes from August to October with values of about 34 mA/m. And another maximum is found during February. Around April and December the CEJ exhibits the smallest values with current densities of about 28 mA/m.

From Figure 3c we can see that the CEJ amplitude shows a distinct longitudinal variation. Generally, the CEJ amplitudes are larger in the Western Hemisphere than in the Eastern Hemisphere. Apart from that, the CEJ amplitudes show smaller undulations with minimum values around $-180°$, $-90°$, $0°$, and $90°$ in longitude. These locations of the minima correspond to the longitudes of the wave 4 peaks in EEJ amplitude (e.g., England et al., 2006; Zhou, Lühr, Alken, & Xiong, 2016).

The dependence of the CEJ amplitude on geomagnetic activity is presented in Figure 3d. It can be seen that the values monotonically get larger when the geomagnetic activity index *Kp* increases. The increase in the CEJ amplitude with *Kp* is nonlinear and follows a quasi-exponential curve. All the large values (>60 mA/m) are found during active periods with $Kp = 7$ and higher.

The increase of CEJ amplitude with magnetic activity is an important characteristic. For that reason we have also checked the relation between the linear index a_P and the CEJ amplitude. For this analysis we have used variable bin sizes of a_P in order to have approximately the same number of events in all the bins. As can be seen in Figure 4a there exists a remarkably good linear relation between a_P and the amplitude. From the regression line we can see that an increase of a_P by 2 nT enlarges the CEJ peak current density by 1 mA/m. This direct dependence on magnetic activity has to be kept in mind in the analysis of other dependences.

For deriving the dependence of the CEJ amplitude on solar radio flux level we have restricted the CEJ sample to magnetically quiet times ($Kp < 2.5$). Throughout the solar cycle there may be a correlation between magnetic and solar activity. In contrast to the dependence on magnetic activity, we can see that the CEJ amplitude shows no clear dependence on the radio flux index *P10.7* in the range from 70 to 200 sfu, as can be
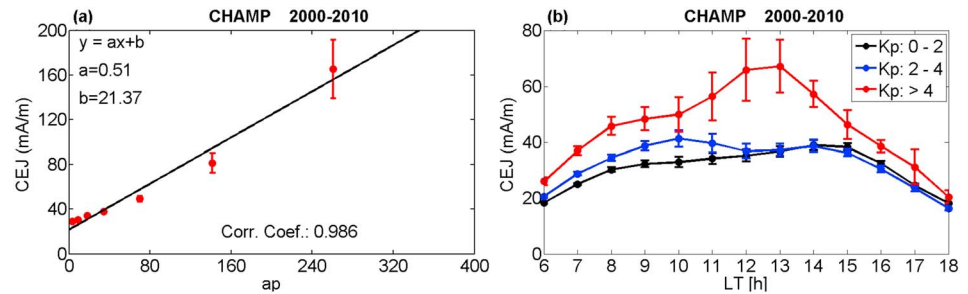
Figure 4. Dependence of CEJ amplitude on magnetic activity. (a) Variation of the CEJ amplitude with a_P index. The red dots denote the mean values of the CEJ amplitudes within each a_P bin. Here a_P is grouped in bins with borders: 0, 6, 12.5, 25, 50, 100, 200, and 400 nT. The function for the regression line is presented in the top left corner. (b) Diurnal variation of the CEJ amplitude separately for three magnetic activity levels. The vertical bars denote the uncertainties of the mean values. CEJ = counter equatorial electrojet.

seen in Figure 3e. Just for $P10.7 > 220$ sfu we observe an increase in amplitude. A possible explanation for that will be offered in section 4.4. Here the smoothed solar flux index $P10.7$ is used and calculated as $P10.7 = (F10.7 + F10.7A)/2$, where $F10.7A$ is the 81-day average of the daily $F10.7$ value.

In earlier publications (e.g., Rastogi, 1974b) it has been mentioned that the CEJ also depends on the phase of the moon. We have investigated such a relation. For obtaining the moon phase, we first calculated the new moon epochs in Modified Julian Day (MJD) after 1 January 2000, 00:00 UT. The formula we used is given in Lühr et al. (2012),

$$\text{MJD}_{\text{NM}-2000} = 5.597 + 29.53058886N - \left(133 \times 10^{-12}\right)N^2 \tag{1}$$

where N is the sequence number of new moons after 1 January 2000, and $\text{MJD}_{\text{NM\_2000}}$ is the time in MJD for each new moon epoch. By increasing N from 0 to a given number, the MJD value for each new moon epoch can be calculated. Then the time interval between two continuous new moon periods is divided evenly into 24 parts, which are termed as moon phase in hours. The new (full) moon occurs when the moon phase is 0 hr (12 hr). As shown in Figure 3f, the CEJ amplitude variation with the moon phase is calculated in intervals of 1 hr. The smallest amplitude of about 30 mA/m is found near new moon epoch. At the moon phase 06 hr the CEJ attains largest amplitudes (33 mA/m). And a maximum is also found near 16 hr. These results indicate that largest CEJs occur around half-moon epochs.

3.2. Average Characteristics of the CEJ Occurrence Frequencies

Having seen the characteristics of the CEJ amplitude, we now want to take a look at the dependence of the CEJ occurrence rates on the various parameters. In this study the CEJ occurrence rate is calculated as the ratio of the CEJ events with respect to the number of total satellite passes providing reliable EEJ profiles for each bin. Here all the EEJ (CEJ) events are considered where the peak amplitude of current density is larger than 10 mA/m and the peaks occur within ±1° QD latitude. Figure 5 presents the dependences of the CEJ occurrence rates on the same set of parameters as in Figure 3. In Figure 5a the local time variation of the CEJ occurrence rate is shown. Highest CEJ rates with values exceeding 38% are observed from 0600 to 0800 LT. Especially around 0600 LT in almost all cases a westward current is encountered. Lowest CEJ occurrence rates of less than 4% are found around noon from 1100 to 1200 LT. Subsequently, a shallow secondary maximum appears at 1600 LT with a value of about 21%.

The CEJ occurrence rate exhibits a prominent seasonal variation, as shown in Figure 5b. One can see that maxima appear around January and July with values exceeding 21%. Minima in occurrence rate are found in April and December. There seems to be a certain similarity in the seasonal variation between amplitude and occurrence rate.

Figure 5c depicts the longitudinal variation of the CEJ occurrence rate. It is clear that the rates are generally larger between −60° and 60° in longitude than in other sectors. Here again we find a superimposed undulation with four local minima located around −165°, −90°, 0°, and 90° in longitude. These correspond well with the wave 4 signal in CEJ amplitude (see Figure 3c).
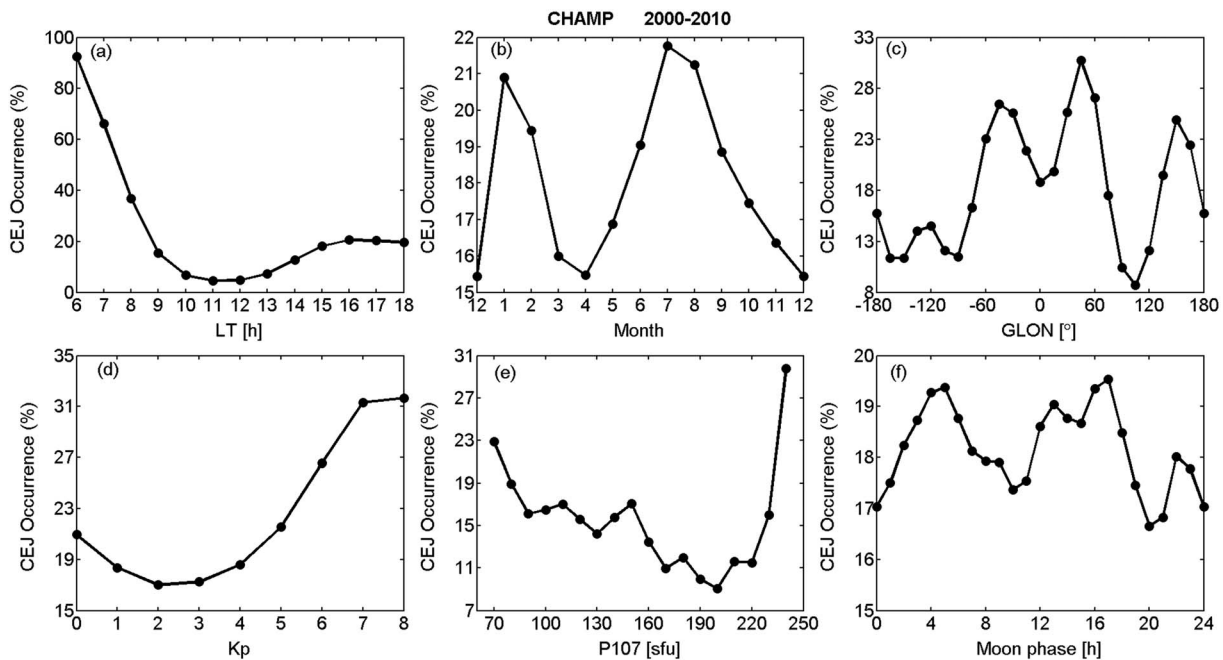
Figure 5. The same as Figure 3, but for the CEJ occurrence rate dependence. CEJ = counter equatorial electrojet.

Figure 5d shows the dependence of CEJ occurrence rate on the Kp index. It indicates that the number of CEJs slightly decreases for quiet times with the growth of Kp up to $Kp = 2$. In case of more active times ($Kp \geq 3$) the CEJ occurrence rate gets larger with increasing geomagnetic activity, doubling up at $Kp = 7$–8. This again confirms the preference of more active times.

An interesting question is the dependence on solar activity. Here again the analysis has been restricted to magnetically quiet times; see above. As indicated in Figure 5e, the CEJ occurrence rate decreases drastically with the increase of the $P10.7$ index. The rate reduces to less than half for $P10.7$ values from 70 to 220 sfu. The reason for the sharp rise in frequency at highest solar radio flux values will be addressed in section 4.4.

In Figure 5f we present the modulation of the CEJ occurrence rate by the moon phase. Peak rates appear around 05 and 17 hr in moon phase. This feature of wavenumber 2 (WN2) pattern is similar to the CEJ amplitude variation with moon phase, as shown in Figure 3f. There actually seems to be an influence of the moon on CEJ occurrence probability.

3.3. Solar Tidal Analysis of the CEJ Occurrence

As reported in previous publications the EEJ intensity exhibits prominent wave-like longitudinal patterns, which are usually attributed to the influence of solar tidal components (e.g., England et al., 2006; Lühr et al., 2008; Lühr & Manoj, 2013; Xiong et al., 2014; Zhou, Lühr, Alken, & Xiong, 2016). Considering the close connection between EEJ and CEJ, we attempt to investigate the solar tidal properties of the CEJ occurrence in this study. Since the tidal characteristics in the EEJ vary with season, we perform separate analyses for the four seasons, June and December solstices as well as the March and September equinoxes. The approach is the same as described in previous publications (e.g., Zhou, Lühr, Alken, & Xiong, 2016; Zhou et al., 2018).

Figure 6 presents the distribution of the CEJ occurrence rate in local time versus longitude frames separately for the four seasons. The diurnal and longitudinal variation of the CEJ occurrence is quite evident in Figure 6a. It is visible in all four seasons that the CEJ events preferably occur in the morning and evening sectors, as mentioned in section 3.2. In addition to these general features the CEJ occurrence rate exhibits several local maxima and minima in certain longitudinal regions. In order to make them more visible, we remove the zonal averages for each hour in LT and obtain the mean free CEJ occurrence rate distribution (see Figure 6b). Actually, the dominating migrating tidal components are suppressed by this procedure. Based on the obtained mean free CEJ occurrence patterns, shown in Figure 6b, we suggest a set of major nonmigrating
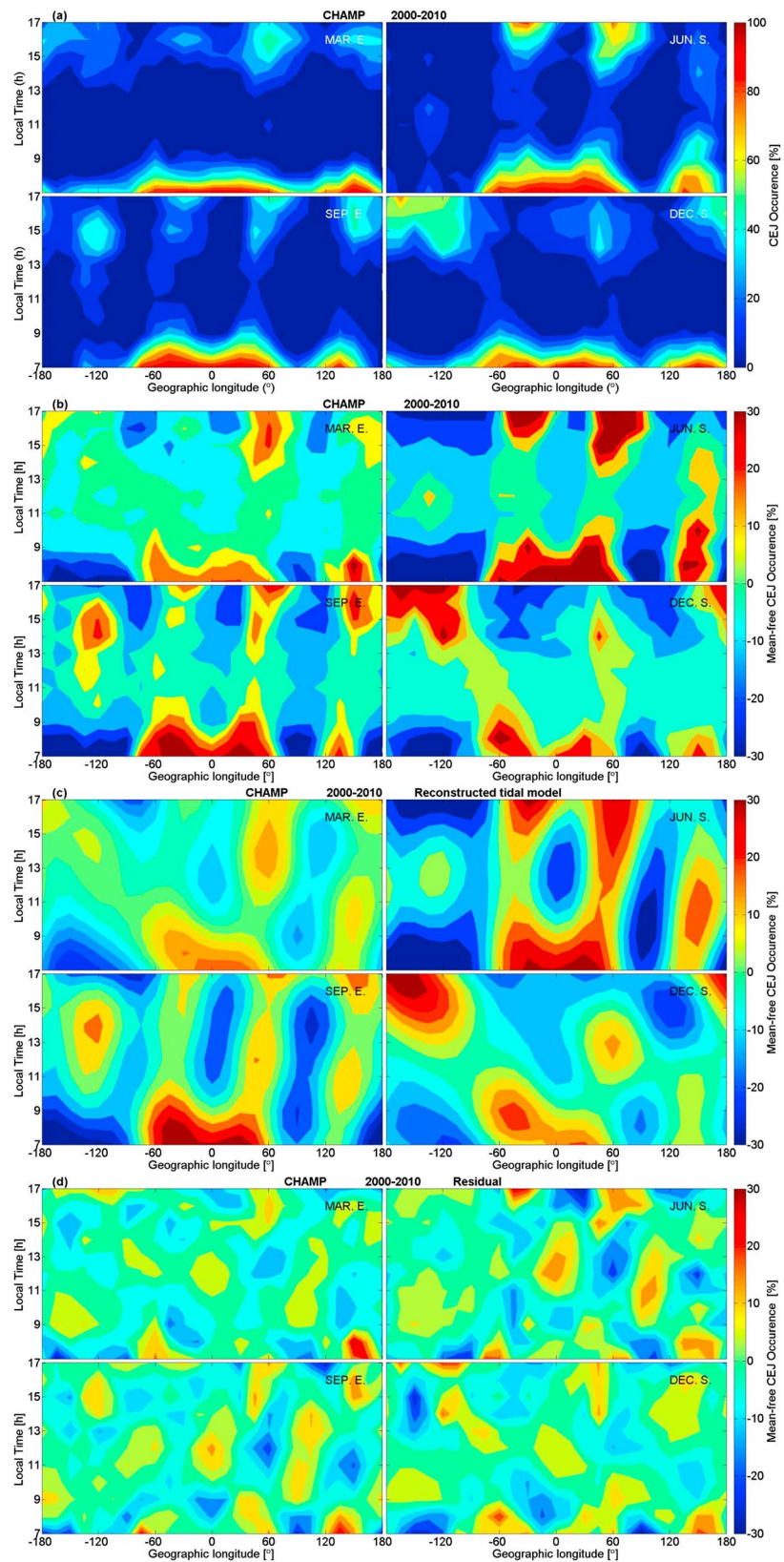
Figure 6. Distribution of the CEJ occurrence rates in local time versus longitude frames, separately for the four seasons. (a) Distribution of occurrence, (b) the mean free occurrence rates, (c) the patterns reconstructed by a tidal model, and (d) the residuals between observation and model. CEJ = counter equatorial electrojet.

Table 1
Results of the Solar Tidal Variation (Amplitude and Phase) of the CEJ Occurrence Rate

Tidal components	Jun		Dec		Mar		Sep	
	Amplitude (%)	Phase (hr)	Amplitude (%)	Phase (hr)	Amplitude (%)	Phase (hr)	Amplitude (%)	Phase (hr)
DE3	5.08	21.2	3.38	19.8	1.95	21.8	7.45	21.97
DE2	9.21	1.6	3.91	0.5	4.83	2.0	4.03	2.3
S0	6.29	9.3	2.31	11.5	2.49	10.2	3.63	9.6
SW1	8.68	5.5	3.72	8.8	1.50	5.1	6.82	6.1
SW3	12.92	7.1	13.74	9.8	9.49	8.6	18.71	8.1
SW4	3.51	6.1	9.70	5.8	5.34	5.8	4.72	4.7
TW4	3.40	5.3	11.22	14.4	6.46	6.2	12.79	5.5
SPW1	14.82	30.7°	2.25	169.2°	5.20	62.5°	8.92	30.2°
SPW2	7.00	158.5°	3.24	21.4°	2.42	171.7°	3.59	158.5°
SPW4	7.84	53.8°	1.33	30.7°	2.80	59.6°	4.60	51.8°

Note. The phase represents the local time at which the tidal wave crest passes the Greenwich meridian. In case of stationary waves, SPWs, the longitude of the maximum is listed. CEJ = counter equatorial electrojet.

tidal components (listed in Table 1) that modulate the CEJ. Then we fit the local time and longitudinal distribution of the CEJ occurrence in each season to the listed tidal components. The patterns of the reconstructed tidal model are shown in Figure 6c. By comparing them with the observation, the residuals can be obtained (see Figure 6d). The completeness of tidal component estimates is verified by checking the residuals for systematic features. Here we find only randomly distributed features in Figure 6d, which confirm our choice. The results of successfully modeled tidal compositions, both the tidal amplitudes and phases, are listed for the four seasons in Table 1.

According to Table 1, for June solstice the stationary planetary wave SPW1 and the semidiurnal westward migrating SW3 are the dominating tidal components, which both contribute to the longitudinal wavenumber 1 (WN1) pattern. The amplitudes of SPW1 and SW3 are 14.8% and 12.9%, respectively. The phase of SPW1 varies about 30.7° in longitude and 7.1 hr in LT for SW3. Besides the longitudinal WN1 patterns, the wavenumber 3 (WN3) pattern is prominent, too. This can be attributed to the diurnal eastward propagating DE2 (see Table 1), whose amplitude (phase) is 9.2% (1.6 hr). During December solstice the longitudinal WN1 pattern is mainly coming from the components SW3 and terdiurnal TW4. The amplitudes (phases) of SW3 and TW4 are 13.7% (10 hr) and 11.2% (14 hr), respectively. Additionally, the WN2 pattern is visible (see Figure 6b). For this feature the semidiurnal SW4 takes an important role, whose amplitude is about 9.7%. During March equinox tidal signatures are least prominent. Here also the tidal components contributing to WN1 pattern (SW3 and TW4) are dominating. The amplitudes of SW3 and TW4, both contributing to WN1, are particularly large during September equinox, with values of 18.7% and 12.8%, respectively. These are about 2 times the values of March equinox. Besides the WN1 pattern the CEJ occurrence rates exhibit prominent longitudinal wavenumber 4 (WN4) patterns around September, which can partly be related to the well-known DE3 component, whose amplitude (phase) is about 7.5% (22 hr); also, SPW4 makes significant contributions to WN4. During those months the DE3 component is largest of all the four seasons. It may be reminded here that the average CEJ occurrence rate is 18%. Therefore, the derived tidal amplitudes partly represent a strong modulation of the overall CEJ occurrence frequency.

It is meanwhile well accepted that the diurnal eastward migrating DE3 is driven from below by deep tropical convection in the troposphere (e.g., Hagan & Forbes, 2002). The amplitude of this tidal component, exciting the WN4 pattern, is largest during the months around August (e.g., Lühr & Manoj, 2013; Oberheide et al., 2009). For checking the tidal effects on the CEJ we particularly analyzed this period of the year. Here we consider the 131 days (days of year: 162–292) centered on 15 August and investigate the tidal characteristics in the same way as done before. The results are presented in Figure 7 and Table 2. Compared with Figure 6b, the WN4 longitudinal pattern is already quite clearer in Figure 7a during the August months. The maximum amplitudes of the mean free CEJ occurrence patterns in Figure 7b are stronger around the −60°–60° longitude sector. This is consistent with the average longitudinal pattern in Figure 5c. The appreciable size of the related WN1 pattern is reflected in Table 2. More interestingly, the longitudinal WN4 patterns maximize during that period. As listed in Table 2, the WN4 results from the tidal components DE3 and SPW4, whose
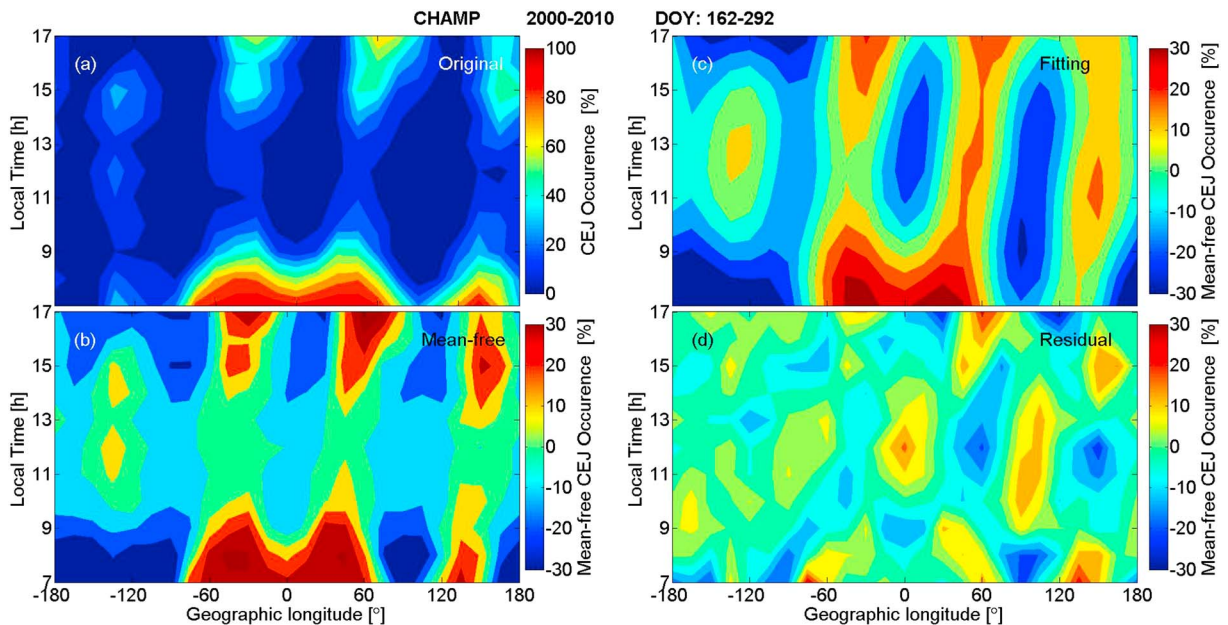
Figure 7. Same format as Figure 6, but for the tidal signatures occurring during the months around August. CEJ = counter equatorial electrojet.

amplitudes are 7.7% and 7.0%, respectively. The phases of these two components are 22 hr in LT and 53° in longitude, respectively. Lühr and Manoj (2013) and Zhou, Lühr, Alken, and Xiong (2016) have reported a phase of the DE3 in EEJ of about 11.5 hr. The phase difference of the DE3 component by about 11 hr indicates that the CEJ events preferably occur at longitudes where the amplitudes of the EEJ are smallest. Similarly, a phase difference of about 40° indicates the same relation between EEJ and CEJ for the SPW4 component.

3.4. Lunar Tidal Analysis of the CEJ Occurrence

Already, Rastogi (1974b) reported a relation between lunar phase and the occurrence of CEJ. As suggested by Stening et al. (1996), the frequency of CEJ events might be influenced by the lunar atmospheric semidiurnal tide. Later it was reported by Stening (2011) that the CEJ events sometimes are frequent around new moon and full moon epochs. For investigating the influence of the lunar tide on the CEJ events, we performed an analysis to investigate the lunar tidal modulation of the CEJ occurrence. The analysis approach is similar to that of the solar tides but replacing the longitude by the moon phase. As reported, the lunar tidal effect on the EEJ is maximal during the northern winter season (e.g., Lühr et al., 2012; Stening, 2011). Thus, for the convenience of comparison with the previous results, we focus our analysis of the lunar tide in the CEJ on the northern winter and summer seasons. Considering the typical occurrence of stratospheric sudden warming events, which also have a pronounced influence on the lunar tidal effect in the electrojet (e.g., Siddiqui et al., 2015; Yamazaki, 2013), we selected 131 days (days of year: 316–080) centered on January 15 to represent the northern winter season, and 131 days (days of year 131–261) centered on July 15 for the northern summer season. During 131 days CHAMP covers just the 24 local time hours.

Figure 8 depicts the CEJ occurrence distribution in LT versus moon phase frames for the two seasons. The frames of Figures 8a and 8b contain, as labeled at the top right corner, the original CEJ occurrence

Table 2
The Same Format as Table 1, but for the Solar Tidal Signatures of the CEJ Occurrence Rate During Months Around August

Tidal components	DE3	DE2	S0	SW1	SW3	SW4	TW4	SPW1	SPW2	SPW4
Amplitude (%)	7.68	6.19	4.27	7.40	16.77	3.13	9.14	12.17	6.12	7.0
Phase (hr)	22.1	2.0	9.2	5.8	7.8	4.3	5.6	34.0°	155.6°	53.2°

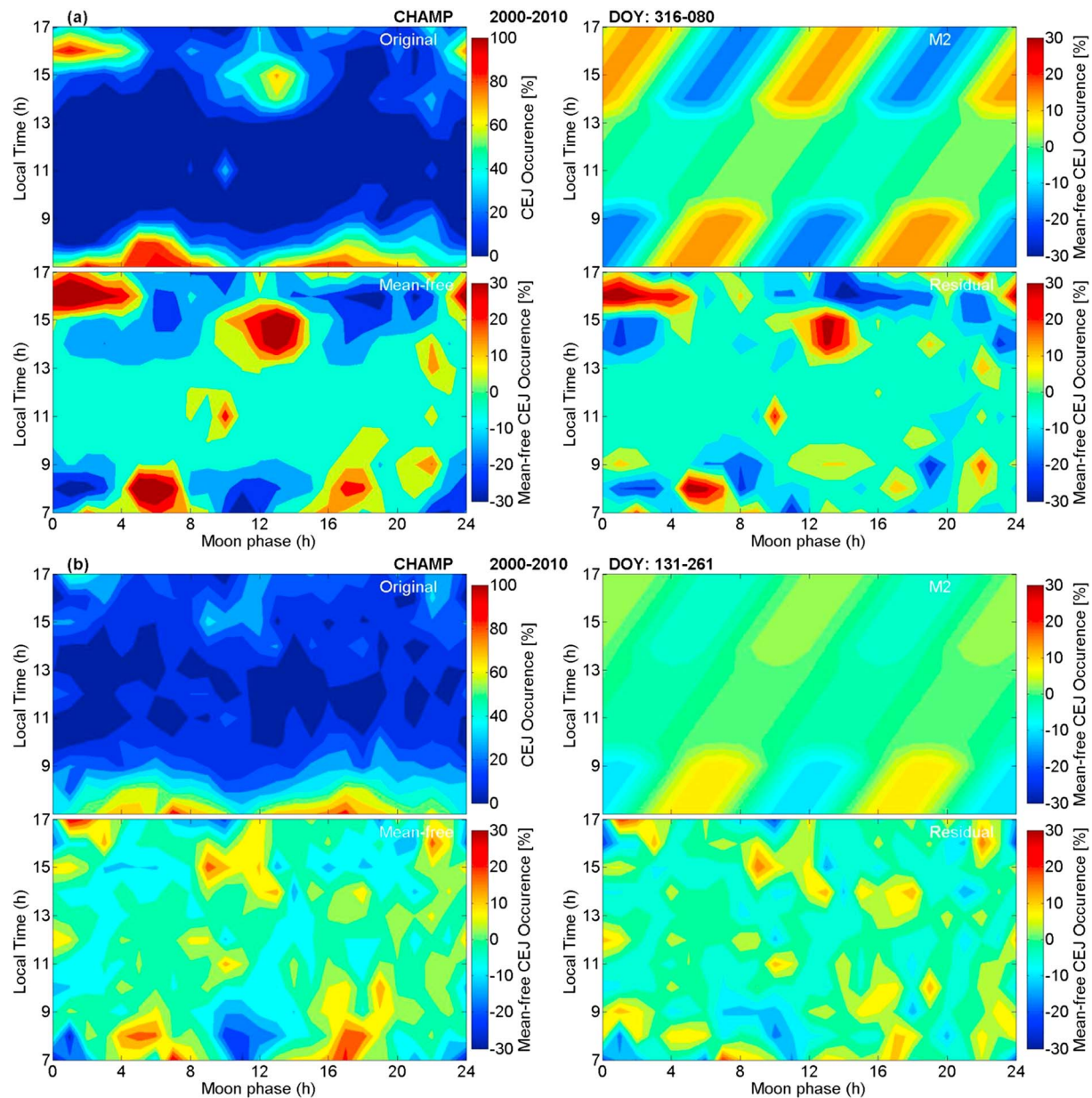*Note.* CEJ = counter equatorial electrojet.

Figure 8. Distribution of the CEJ occurrence rates in local time versus moon phase frames, separately for the months (a) around January and (b) around July. Shown are the original occurrence rates, the mean free occurrence rates, the patterns reconstructed by a tidal model, and the residuals between observation and model. CEJ = counter equatorial electrojet.

distribution, the mean free CEJ occurrence rates, the semidiurnal lunar tidal component (M2) fitted to mean free occurrence rates, and the residuals between the mean free observations and the modeled M2. For both seasons we find in the original observations the typical diurnal variation with many events at morning and evening and an occurrence rate close to 0 around noon. After removal of the mean value over all moon phases for each hour in LT interesting features appear. During winter season the evening CEJ events are frequent shortly after new moon (0–3 hr) and full moon (12–14 hr), while the morning CEJ events show higher occurrence rates around 06 and 17 hr in moon phase. Around noontime the CEJ events are quite rare but show two maxima, at 10 and 22 hr in moon phase. All these patterns are consistent with the M2 lunar tide. To obtain quantitative results, we fitted a M2 tidal model to the observations. In order to account for the general change in CEJ occurrence rate over a day, independent M2 fitting analyses were performed for the three

Table 3
Amplitude and Phase Values of the Lunar M2 Tide in the CEJ Occurrence for Northern Winter and Summer Seasons

Local time sectors	Northern winter		Northern summer	
	Amplitude (%)	Phase (hr)	Amplitude (%)	Phase (hr)
0700–0900 LT	17.2	1.9	10.0	2.2
1000–1300 LT	3.2	2.2	2.4	3.1
1400–1700 LT	15.5	2.6	4.6	3.6

Note. Results are given for three different local time sectors. The phase represents the local time, at which the M2 tidal wave crest appears at new moon or full moon. CEJ = counter equatorial electrojet.

local time ranges (0700–0900 LT, 1000–1300 LT, and 1400–1700 LT). The obtained tidal signature of this best fit model is shown in the top right frame of Figure 8a, and numerical values of the amplitude and phase of the CEJ occurrence rate modulation by the M2 lunar tide are listed for the different local time ranges in Table 3. The residuals contain still some prominent features but no M2 signals. It is interesting to note that the phase of the M2 lunar tide exhibits some slight variations, increasing through the three time intervals and amounts on average to 2.2 hr in LT during the northern winter season. This is equivalent to saying that the crests in CEJ occurrence rate appear at noon around the moon phases at 10 and 22 hr. These phase values are consistent with the lunar times reported by Rastogi (1974b) for the evening and morning CEJs at Huancayo. The largest amplitudes of M2 are found in the morning with occurrence rates of 17%, and 15.5% for the early evening CEJs. Around noon the amplitude is small but still significant.

For the northern summer season the lunar tidal analysis results are presented in Figure 8b. The lunar tidal characteristics are quite similar to that in winter but exhibit smaller amplitudes, especially during the 1400–1700 LT sector. In the mean free distribution there is already some M2 tidal signal discernable. The fitted M2 model largely confirmed the impression. Both the color map in the top right frame of Figure 8b and the numbers in Table 3 reflect the modulation of the occurrence rates by M2 but with reduced amplitude, for example, one third of the winter level during 1400–1700 LT. The phase values are somewhat larger but also increasing with LT. The mean value infers that the M2 crest in CEJ occurrence rate appears about 1 day earlier in summer than in winter.

In summary we may state that the lunar M2 tide is an important factor during the northern winter months in modulating the occurrence rate of CEJ events. During other parts of the year the influence of M2 is also present but at a reduced level.

3.5. Response to Changes in Solar Wind Input

It has been reported in earlier studies that the orientation of the IMF can have an influence on the equatorial electrojet. For checking the CEJ response to changes of solar wind input, we use the superposed epoch analysis. The Newell coupling parameter (Newell et al., 2007) is chosen for representing the energy input from the solar wind. This coupling parameter has been rescaled for representing the merging electric field at the magnetopause (e.g., Xiong et al., 2016; Zhou, Lühr, Xiong, & Pfaff, 2016) and is defined as

$$E'_m = \frac{1}{3000} V_{\text{SW}}^{\frac{4}{3}} \left(\sqrt{B_y{}^2 + B_z{}^2} \right)^{\frac{2}{3}} \sin^{\frac{8}{3}}\left(\frac{\theta}{2}\right) \tag{2}$$

where V_{sw} is the solar wind velocity in km/s, B_y and B_z both in nanotesla are the IMF components in geocentric solar magnetospheric coordinates, and θ is the clock angle of the IMF. With these units the value of merging electric field will result in mV/m, comparable in size with the solar wind electric field. It is necessary to consider a memory effect of the magnetosphere-ionosphere-thermosphere system to changes of the solar wind input. Following the arguments of Richmond et al. (2003), the weighted merging electric field is integrated over a period of time. Details of the approach we used can be found in the publication of Xiong et al. (2016)

$$E_m(t, \tau) = \frac{\int_{t_1}^t E'_m(t') e^{(t'-t)/\tau} dt'}{\int_{t_1}^t e^{(t'-t)/\tau} dt'} \tag{3}$$

where, E'_m is merging electric field and treated as a continuous function of time t'; t_1 is chosen 3 hr before the actual epoch, and τ is the e-folding time of the weighting function in the integrands, with a value $\tau = 0.5$ hr. Based on the resulting time-integrated merging electric field (Em), we search for events of solar wind sudden input changes where the increase of Em exceeds 0.7 mV/m within a time span of 15 min. In the applied superposed epoch analysis the times when Em shows a step-like increase are used as the key
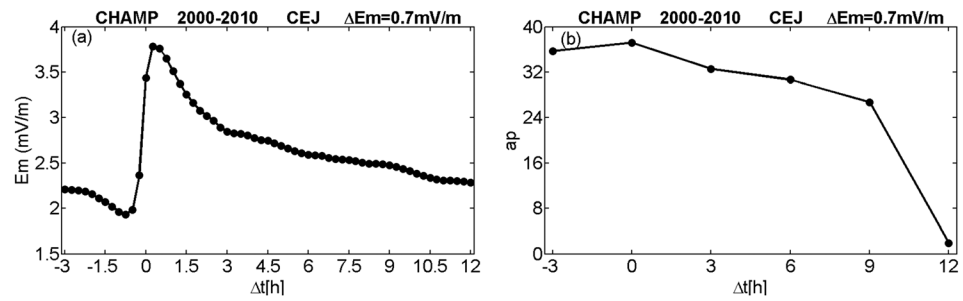
Figure 9. The average temporal evolution of (a) the merging electric field Em and (b) the magnetic activity a_P index after a sudden increase of solar wind input for all the events that are accompanied by a CEJ event. CEJ = counter equatorial electrojet.

time, namely, $\Delta t = 0$ hr. During the 10 years of interest 3,182 time series of Em with sudden increases were detected, which contained at least on one orbit a CEJ event. The average temporal evolution of all the stacked Em curves is shown in Figure 9a. For comparison the corresponding average magnetic activity evolution represented by the a_P index is added in Figure 9b. The time period we considered ranges from 3 hr before to 12 hr after the key time with a resolution of 15 min for Em and 3 hr for the a_P index. At the key time, a sudden increase of about 2 mV/m in Em can be observed in Figure 9a, reaching a peak value of about 4 mV/m. Thereafter Em decreases quite rapidly for 3 hr and then more gradually until reaching preevent levels at $\Delta t = 12$ hr. From Figure 9b we see that events occur during times of enhanced magnetic activity, as reflected by the a_P index ranging on average between 30 and 40 nT. Only 9 hr after the key time it decays to quiet levels.

Of interest here is the evolution of equatorial current density after the sudden increase in solar wind input. CHAMP provides only one snapshot of the electrojet on every orbit. Therefore, the time series of CEJ current profiles at the magnetic equator from all the relevant events are stacked relative to the key time and sorted into 90-min-long (orbital period) bins. More details about the applied superposed epoch analysis can be found in the publication of Xiong et al. (2016). Figure 10 shows the evolution of CEJ occurrence rate after a sudden increase of solar wind input separately for four different local time sectors. For determining the rates the superposed epoch analysis has been applied equally to CEJ and EEJ events and subsequently the ratio in
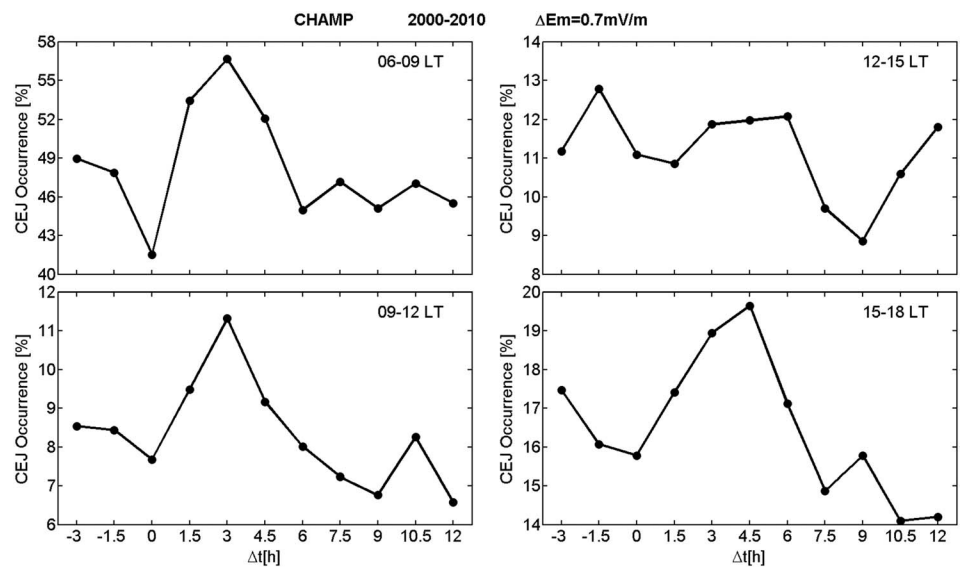

Figure 10. Superposed epoch analysis of the CEJ occurrence rate in response to a sudden increase of solar wind input at the key time ($\Delta t = 0$ hr). The temporal evolution of the CEJ occurrence rate is shown for different local time sectors. CEJ = counter equatorial electrojet.
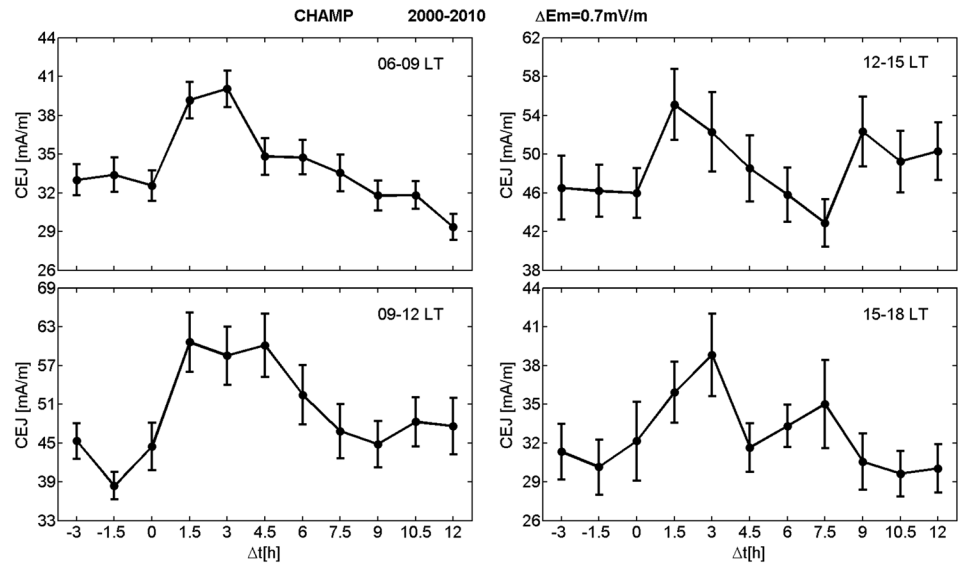
Figure 11. The same as Figure 10, but for the amplitude of the CEJ peak current density. The black bars denote the uncertainties of the mean values. CEJ = counter equatorial electrojet.

each Δt bin calculated. An obvious feature in the four frames is the peak in occurrence rate about 3 hr after key time. Around the key time we find a reduction of the rate. Both these features are consistent with the expected evolution of the ionospheric electric field. Right after the increase in solar wind input commonly an eastward pointing prompt penetration electric field is set up at daytime, lasting about an hour. This suppresses the formation of CEJ. After a few hours the disturbance dynamo will set up a westward electric field (Fejer & Scherliess, 1995) that peaks at the equator with a delay of about 3 hr. Such a zonal E field is in favor of causing CEJs.

Additionally, the CEJ amplitude response to an Em step-like change is also studied. Figure 11 presents the average evolution of the CEJ amplitude after the sudden solar wind input. Here again we show the results separately for the four local time sectors and at a resolution of 1.5 hr. Black bars at each point indicate the uncertainty of the average values. Here the uncertainty is defined as $\sigma/\sqrt{n}$, where σ and n are the standard deviation and the number of events in each Δt bin, respectively. A common feature of the CEJ amplitude is a peak in the range $\Delta t = 1.5 - 4.5$ hr. This average increase of about 20% can probably be related to the effect of the disturbed wind dynamo. The westward electric field generated by this dynamo does not only increase the probability for CEJs but also their amplitudes. Conversely, the eastward pointing prompt penetration E field causes obviously only a minor depression of the CEJ amplitude in the time range around $\Delta t = 1.5 - 4.5$ hr. It is worthy to note that the initial amplitudes before the key time are well above the average levels of the respective LT sectors (cf. Figure 3). This is an indication that step-like events are embedded in a period of enhanced activity, as confirmed by the a_P curve in Figure 9.

4. Discussion

As mentioned in parts of section 1, there are several questions about the mechanism and variability of CEJ, although it has been studied extensively for several decades. This was to a good part due to sparse and patchy observations by a limited number of magnetic observatories under the magnetic equator. As a consequence, spatial and temporal variations could not be separated effectively. Many processes that favor the occurrence have been addressed in the past but without providing the full picture. In order to improve the situation, we make use of the globally distributed and continuous magnetic field sampling of the CHAMP satellite over the years from 2000 to 2010. This unprecedented data set of electrojet profiles, covering nearly a solar cycle, allows to derive the climatological properties of the CEJ and its dependences on many controlling parameters.

4.1. Driving Mechanisms of the CEJ

Before presenting the statistical properties of the CEJ we shortly want to introduce the important drivers for causing a westward current at the equator. Generally, large-scale tidal winds generate a polarization electric field at low latitudes that points eastward during daytime and westward at night. The switch in direction occurs in the morning around 0700 LT and after 2000 LT in the evening (e.g., Fejer et al., 2008). This background field is the main driver for the electrojet. In addition, more local zonal winds also make contributions to the current density distribution. Eastward winds in the E layer (95–115 km) cause eastward currents, while such winds at altitudes above 120 km drive westward currents at latitudes poleward of about 3° QD latitude. Another relevant factor is the E field penetrating from auroral latitudes to low latitudes. These are commonly transient effects reflecting solar wind-magnetosphere interaction.

It is primarily the interplay of these main drivers that decides whether the net electrojet current flows eastward or westward. Consequently, there is no simple rule for predicting the occurrence of a CEJ. But it can generally be stated when the large-scale dawn-to-dusk E field is weak the other two drivers, for instance, the dynamo electric field and the local zonal wind have an easy game to cause a westward current flow. In a statistical study Stolle et al. (2008) compared E fields from 150 km altitude echoes, derived by the JULIA (Jicamarca unattended long-term studies of the ionosphere and atmosphere) radar, with EEJ recordings at Huancayo. Their data set covered the years 2001–2006 and is limited to events from quiet times ($Kp < 3$). They obtained a good linear relation between vertical plasma drift velocity and Huancayo northward deflections with a correlation coefficient of 0.83. Interestingly, CEJs are accompanied by small but eastward electric fields, on average less than 0.2 mV/m. Hardly any of their considered CEJ events during daytime (0800–1600 LT) was accompanied by a westward E field at 150 km altitude. This provides strong evidence that the distribution of local winds in the E layer is responsible for CEJs during quiet times. In the subsequent sections we will discuss the average dependences of CEJs on the various parameters one by one.

4.2. Diurnal Variation of CEJ

The CEJ occurrence probability varies drastically over the course of a day (cf. Figure 5a). Around 0600 LT in the morning in almost all cases we observe westward currents. This is consistent with the report of Cohen and Achache (1990) based on Magsat observations. At this time of the day the background E field is still pointing westward, therefore dominating the current direction. During the following hours the large-scale eastward E field more and more controls the flow direction. Around noon the CEJ occurrence rate is down to 4%, well below the average value of 18%. It is obviously hard for the other drivers to compete with the background E field at that time. Toward evening hours average CEJ occurrence frequencies are achieved. Based on Ørsted observations Vichare and Rajaram (2011) have also investigated the local time variation of CEJ occurrences. In their Figure 9 the highest occurrence probability appeared around 1200–1300 LT. We cannot confirm this surprising result, but their data set covered only a limited range of local times.

The average amplitude of CEJ shows a quite different diurnal variation (cf. Figure 3a). Here we find largest values around noon. The current density is proportional to the product between the effective E field and the conductivity. The conductivity of the E region varies to first order as the square root of the cosine of the solar zenith angle. However, the CEJ amplitude varies less over a day than the conductivity, inferring that on average the net westward E field is smallest around noon. This is consistent with the very low occurrence probability for CEJ at that local time.

4.3. CEJ Dependence on Magnetic Activity

It is known that the EEJ intensity is reduced during magnetically active periods. During those times the large-scale background electric field is perturbed, and other influences like E fields penetrating from high latitudes or resulting from the disturbance dynamo wind can cause counter electrojets. On Figure 5d we find occurrence frequencies varying around the mean value of 18% up to $Kp = 4$. For higher activity the rates are increasing and almost double up at $Kp = 8$.

Even more interesting is the dependence of the CEJ amplitude on magnetic activity. We find a monotonic increase toward higher activity (cf. Figure 3d). For example, the linear relation between the CEJ amplitude and the a_P index (see Figure 4) has never been mentioned before. It is probably the E field driven by the disturbance dynamo that causes the strong westward current densities surmounting partly 160 mA/m. In addition, also the conductivity may increase during higher activity. Interestingly, the regression line in

Figure 4a does not start at 0 but at amplitudes around 20 mA/m. This quiet-time bias value represents obviously the effect of other drivers (e.g., tides) that are not dependent on activity.

The increase in CEJ amplitude with magnetic activity is not distributed evenly over local time. From Figure 4b we can conclude that for moderate activity (Kp = 2–4) the CEJ amplitudes mainly increase during the hours before noon. For magnetically very active periods this morning trend prevails, but particularly large amplitudes are found around noon. Studies of the disturbance wind (e.g., Xiong et al., 2015) show that at the equator the westward component is large at early morning and decays toward noon. This is consistent with the observed preferred of CEJ amplitude increase in the morning compared to afternoon and evening hours. At times of very high magnetic activity the disturbance wind lasts to later LT hours and even stays westward for almost the whole day (see Figure 6 of Xiong et al. (2015)). Together with the peak in conductivity, the large amplification around noon can thus be explained.

4.4. CEJ Dependence on Solar Radio Flux

In the previous section we showed the clear dependence of CEJ amplitude on magnetic activity. In case of solar activity a rather different picture emerges. Here we find for low solar flux levels like $P10.7$ = 70 average occurrence rates of some 20%, which reduce to less than 10% around $P10.7$ = 220 sfu. The preferred appearance of CEJ around solar minimum years has earlier been reported by other groups, for example, Hutton and Oyinloye (1970) and Marriot et al. (1973, 1979). During times of high solar flux the EEJ develops large amplitudes. Alken and Maus (2007) have shown that the EEJ intensity varies approximately as the square root of $P10.7$. That means it is harder for local winds or additional electric fields to reverse the currents during solar maximum years. For very high solar fluxes a steep increase of occurrence rate is found in Figure 5e. A closer inspection reveals that all these observations come from December solstice months of 2001. Thus, they are not representing actual annual means and seemed to be affected by seasonal and local time biases.

The amplitude of CEJ events shows, different from the occurrence rate, on average only an insignificant dependence on solar flux (cf. Figure 3e). This may be surprising since the ionospheric conductivity clearly increases with $P10.7$. Obviously, the winds, which are mainly responsible for the CEJ during quiet times (here events are limited to $Kp < 2.5$), do not vary much with solar activity. Unfortunately, winds at E layer altitude are difficult to measure; therefore, our suggestion has to await later observational confirmation. Just at early morning, when the background E field is still pointing westward, the amplitude of CEJs increases with solar activity. This has also been observed before, for example, by Gouin and Mayaud (1967), but it is related to a somewhat different CEJ mechanism than during daytime. During these early morning hours the large-scale polarization E field is still pointing westward, and high solar fluxes enhance the conductivity. The larger amplitudes found at very high $P10.7$ values can again be explained by the confinement of these few cases to 2001 December solstice months.

4.5. The Latitudinal Width of CEJ

The equatorial electrojet is known to be a narrow ribbon of enhanced current density. Here we have used the peak current density for representing the intensity. However, the total current is proportional to the product between latitudinal width and peak amplitude. Thus, for completeness we analyzed also the variation of the CEJ HMW. On average we obtain for the CEJ a value for HMW of 5.2° in latitude. This is about 1° more than the average HMW of the EEJ. Already, Tomás et al. (2008) noticed that the CEJs occurring in connection with solar eclipses are significantly wider than the previously existing EEJ. It was evident in their cases that the reverse current EEJ sidebands (see Zhou et al., 2018) became part of the westward current channel, making it extra wide.

The top row of Figure 12 shows the dependence of HMW on local time and magnetic activity. The dependences of HMW on the other parameters, as used in Figures 3 and 5, are insignificant. The diurnal variation, shown in Figure 12a, exhibits a clear peak in width around noon. Toward morning and evening the width gets smaller by about 1°. For the dependence on magnetic activity we observe a steady increase with Kp (see Figure 12b). Starting at 4.5° for Kp = 0 the average value of HMW reaches 6.5° at Kp = 8. From Figures 3 and 4 we know that the CEJ amplitudes get large with increasing disturbance level. Obviously higher current densities are also accompanied by a larger width. This inference is also true for the diurnal variation. The wider CEJs at noon are accompanied by larger amplitudes around midday (cf. Figure 3a). Toward morning and evening hours both amplitude and width become smaller. A possible explanation for the enhanced
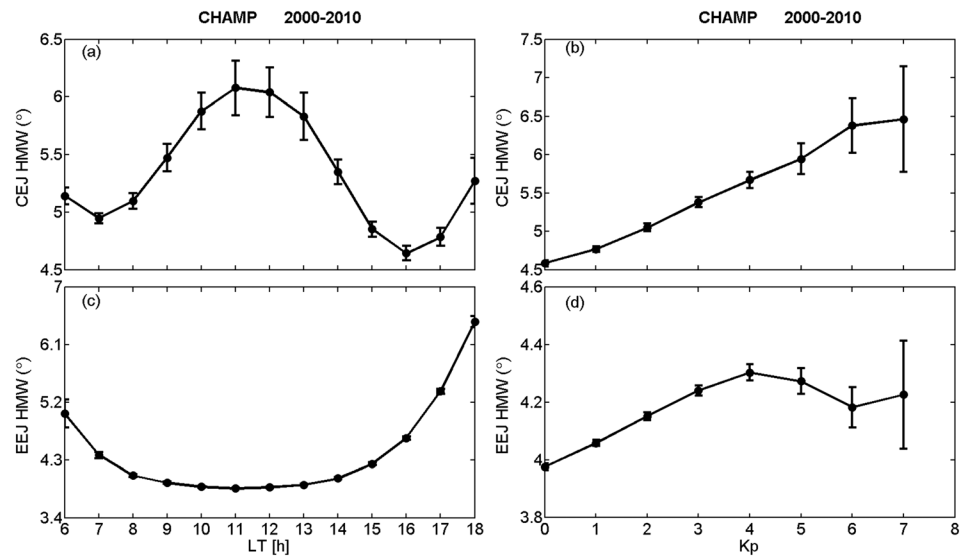
Figure 12. Dependences of the CEJ and EEJ current profiles' half-maximum widths (HMW) on local time (a and c) and *Kp* index (b and d). The black bars denote the uncertainties of the mean values. CEJ = counter equatorial electrojet; EEJ = equatorial electrojet.

total CEJ current strength could be a thicker *E* layer. That would allow for a Cowling channel wider in latitude and a larger height-integrated current density for a given zonal *E* field. In situ measurements are recommended for validating that suggestion.

For comparison, the dependence of the EEJ width on various parameters was also analyzed. Figures 12c and 12d show the diurnal and *Kp*-dependent HMW variations. Interestingly, the EEJ exhibits a variation with local time quite different from that of CEJ. Larger widths are found in the evening and morning hours, just the times when the amplitudes are small. The narrower width of the EEJ is primarily controlled by the reverse current sidebands. These westward current features are driven by zonal winds at altitudes above 120 km. Toward the terminator sectors the sidebands move to higher latitudes (appr. 7° QD latitude; see Zhou et al., 2018). Opposed to the conditions for CEJ, the magnetic activity does not have a significant influence on the EEJ width.

4.6. Seasonal Variation of CEJ Occurrence Rate

Over the course of a year the CEJ occurrence frequency shows a significant variation with a primary maximum during late summer (July–August) and a secondary peak at January (cf. Figure 5b). Minima appear around April and December. Similar distributions of CEJ occurrence rates have been reported earlier (e.g., Marriot et al., 1973, 1979; Mayaud, 1977; Vichare & Rajaram, 2011). An interesting suggestion for the summer maximum comes from Vineeth et al. (2016), claiming that the occurrence of CEJ can be favored by the ablation of meteor trails. We tried to verify that idea and looked for reports on meteor trail count rates. Haldoupis et al. (2007) showed in their Figure 3 the average daily meteor counts for the years from 2000 to 2005. Lowest count rates are encountered around February–March. Thereafter the rates increase, reaching double the counts of minimum at the peak in July. Subsequently, the curve declines more gradually toward the late winter minimum. All these characteristics are well reflected by the CEJ occurrence curve for the months from April to December, strongly supporting the influence of meteor trails. Just the peak at January does not fit this explanation. Further down we will offer an explanation for that.

Vineeth et al. (2016) argued that a dust layer is produced in the lower part of the *E* layer by meteoric ablation. The attraction of electrons by dust particles causes a downward electric field and thus a westward current in the bottomside *E* region. Such a current would reduce the magnetic effect of the eastward EEJ. Our observations are in favor with the inferences of a close correlation between meteor count rate and CEJ occurrences. With our data we can, however, go one step further. When looking at the longitudinal distribution of CEJ occurrence rates during late summer months (highest meteor count rates) we find large values primarily in

the sector −60° to 150° longitude (see Figure 7). Over that range the magnetic equator is located in the northern (summer) hemisphere. Obviously, the lower solar zenith angle in that hemisphere seems to amplify the electrodynamic effect of the ablated dust. More studies are required for clarifying the role of the related currents.

We also observe a CEJ occurrence peak in January. For that meteors cannot be accounted for. Our explanation is that this is caused by the influence of stratospheric sudden warming events, which typically occur around January. In those cases a strong modulation of the electrojet by the lunar tide causes repeatedly CEJs during times of deepest electrojet weakening. More details on that will be presented in the next section.

4.7. Modulation of the CEJ by Tides

The modulation of the electrojet by solar and lunar tides has been the subject of many studies. Conversely, for the CEJ this is much less the case. The tidal component is introduced into the EEJ by winds driven by the atmospheric tides. Their effect adds to the rather stationary large-scale polarization electric field. Forbes and Lindzen (1976) were the first to solve a full three-dimensional, self-consistent model of the equatorial electrodynamics. By introducing diurnal and semidiurnal atmospheric tides they found strongest deviations from the symmetric EEJ curve during late afternoon hours. We may relate, for example, the observed secondary peak in CEJ occurrence rate at 1600 LT (cf. Figure 5a) to these effects of migrating solar tides.

More prominent, however, are the effects of nonmigrating tides. These produce distinct longitudinal patterns. Particularly outstanding in the EEJ are the WN4 patterns (e.g., England et al., 2006; Lühr & Manoj, 2013), which are related to the DE3 tidal component. The close correlation of tidal features between zonal wind in the E region and the EEJ had been demonstrated by Oberheide et al. (2009). Obviously, the tidal winds at lower thermosphere altitudes modulate the electrojet sometimes so much that the current direction reverses. An indication for that can be found in Figures 3c and 5c where four peaks appear in CEJ amplitude and occurrence rate that can be related to DE3. Already, Vichare and Rajaram (2011) reported these four CEJ occurrence peaks at similar longitudes.

We performed a more detailed analysis of the CEJ tidal features, separately for the four seasons. Many components of the EEJ tidal spectrum, which are revealed by Lühr and Manoj (2013), are also prominent in the CEJ (see Figure 6 and Table 1). Interestingly, highest CEJ occurrences are found out of phase with the corresponding tidal signals of the EEJ. This clearly demonstrates that tides are an important mechanism for CEJ generation. For a special analysis of the important effect of the DE3 we focused also on the months around August when the driving by DE3 is strongest (see Figure 7 and Table 2). During that period the WN4 signatures are largest in the CEJ, but still stronger are the components contributing to WN1 (SPW1, SW3, and TW4; cf. Table 2). Numerical experiments with the TIMEGCM model revealed that global scale secondary waves can be excited through nonlinear interaction between tides and planetary waves (e.g., Hagan & Roble, 2001), for example, SW3 = SW2 + SPW1 and TW4 = TW3 + SPW1. In our case this could be modulation of the migrating semidiurnal and terdiurnal tides by the enhancement of the CEJ occurrence rate over a certain longitude range, for example, by the effect of meteor dust. In section 4.6 we mentioned that the meteor effect is largest during late summer and speculate that the effect on CEJ maximizes in the longitude sector where the dip equator lies in the Northern Hemisphere. Within this longitude range all tidal amplitudes are enhanced. Thanks to the coincidence of CEJ amplification by the meteor dust and maximum DE3 driving from below, the overall CEJ tidal wave power is largest during the late summer months. It will definitely require future dedicated studies to confirm the longitudinal dependence of the meteor dust effect on CEJ occurrence.

Besides the solar tides also, the lunar tide has an influence on CEJ. Already, Bartels and Johnston (1940) studied the solar and lunar tidal modulation of the electrojet signal at Huancayo. They found on certain days particularly large lunar-tidal variations, the so-called big-L days, which occurred preferably in January. However, they did not provide any explanation for the responsible mechanisms. By making use of our global-scale data set we looked into lunar tidal signatures in the CEJ occurrence rate. We selected two intervals of about 4 months for the analysis, one centered around 15 January, when the lunar tidal effect is reported to be large, and the other centered around 15 July, as contrast. Figure 8 clearly confirms the preference of the winter months for more pronounced lunar tidal modulation of the CEJ occurrence rate. Quite obviously, the semidiurnal lunar tide M2 is the most prominent. Several authors have reported about the amplification of M2

signatures in the low-latitude ionospheric electrodynamics during stratospheric sudden warming events, which occur preferably during the months December, January, and February (e.g., Chau et al., 2012; Pedatella & Liu, 2013). The strong modulation of the electrojet causes a higher probability for CEJs, which in our view is responsible for the peak in the annual variation at January (cf. Figure 5b).

From Figure 8 it is interesting to note that the lunar tidal signature is larger during morning and evening hours. Already, Rastogi (1974b) noticed the preferred occurrence of CEJs during these LT hours. He correctly stated that the occurrence peaks at these two time sectors appeared at different moon phases, consistent with our observations. We regard the preference of morning and evening CEJ events to first order as resulting from an interaction of the lunar tidal winds with the smaller EEJ background polarization E field during these hours. When comparing the amplitudes of tidal occurrence rate variations between summer and winter in Table 3, we find an increase by about a factor of 1.5 for morning and midday hours, but during the late afternoon the rates increase by more than a factor of 3 in winter. This large factor is mainly caused by the high CEJ rates around 1600 LT shortly after new moon and around 1500 LT shortly after full moon. These outstanding peaks are clearly visible in Figure 8a. Probably they are the reason for the late afternoon humps in amplitude and occurrence rate (cf. Figures 3a and 5a). Our tidal analysis cannot fully explain them. Therefore, they are still outstanding in the residuals (Figure 8a, bottom right). Nothing comparable to these evening features can found during the summer season (cf. Figure 8b).

For getting a better understanding of the reason for the high rates we specially inspected the events. The great majority of CEJ events in the two outstanding late afternoon bins originate from the years 2003 and 2009. During these two years strong stratospheric sudden warming events took place (see, e.g., Siddiqui et al., 2015). This observation provides additional evidence that SSWs are causing more CEJs and thus can be regarded responsible for the occurrence rate peak in January. The stronger CEJs associated with more intense SSW events is also reported by Vineeth et al. (2009). The peaks in CEJ rate, confined to certain local times at epochs shortly after new moon and full moon, may be explained by the constructive interference of solar migrating tides with the lunar M2 tide. The occurrence peaks are co-located with the M2 tidal crest, and Forbes and Lindzen (1976) showed that the solar migrating tides of the atmosphere have the largest effects on the EEJ during late afternoon and evening hours. The absence of such localized evening CEJ occurrence peaks in summer (cf. Figure 8b) we explain by the missing SSW events during that season.

From the derived phase values of the lunar M2 tide we can deduce that the crest of CEJ occurrence appears at 1200 LT around moon phases of 9.8 and 8.9 hr in winter and summer, respectively. Lühr et al. (2012) reported moon phases of 3.8 and 2.3 hr for the noontime passage of the EEJ lunar tidal crest during December and June solstices, respectively. This systematic difference of about 6 hr in lunar phase confirms also for the lunar M2 tide the out-of-phase relation between EEJ and CEJ.

4.8. Effect of Sudden Change of Solar Wind Conditions on CEJ

We regard our analysis of the CEJ response to a sudden increase of solar wind input as an extension of the study by Xiong et al. (2016). For that reason we adapted the same definition for the step-like increase of the merging electric field (Em). While they consider the response of several electrodynamic quantities (ExB drift, EEJ current, zonal wind), we focus just on the CEJ behavior. The figures that can be directly compared are Figure 3a of Xiong et al. (2016) and our Figure 11. Before the step-like change the EEJ amplitudes are reduced by some 15 mA/m, while the current densities of the CEJ are enhanced by about the same amount compared to the quiet-time average value. The reason for both these displacements is the prevailing enhanced magnetic activity during the events (see Figure 9b).

In response to the sudden increase of Em, at $\Delta t = 0$h, the EEJ amplitude immediately jumps up. This can be related to the transient effect of the eastward directed prompt penetration E field, as earlier reported (e.g., Kelley et al., 2003; Kikuchi et al., 1996). Interestingly, there is no significant reduction of the CEJ amplitude observed at that time. But the CEJ occurrence rate exhibits a minimum at the key time (cf. Figure 10) consistent with the appearance of an additional eastward E field.

A rather prominent effect is caused by the disturbance dynamo (e.g., Blanc & Richmond, 1980; Huang et al., 2005) peaking around 3 hr after the sudden increase of solar wind input. The EEJ amplitude is reduced at that epoch, more pronounced during prenoon than afternoon hours (see Figure 3a of Xiong et al., 2016), and the CEJ amplitudes are enhanced around that time by 5–15 mA/m (see Figure 11). Also, here the largest increase

in amplitude is observed shortly before noon. From these direct comparisons between EEJ and CEJ we see that the gains and losses in EEJ amplitude are directly compensated by the CEJ. This infers that the prompt penetration and disturbance dynamo E fields are add-ons to the prevailing large-scale polarization electric fields just shifting the zero line, either favoring eastward or westward electrojet currents.

When looking at the CEJ occurrence rates, the largest increase due to the disturbance dynamo is observed during morning hours, 0600–0900 LT (cf. Figure 10). There appears almost no change in rate during the afternoon hours, 1200–1500 LT. Intermediate amounts of increases are found at prenoon and in the evening. This local time-dependence of disturbance wind effect is comparable with the diurnal variation of CEJ occurrence rates, as shown in Figure 5a.

Also, the gain in amplitude caused by the disturbance dynamo wind is depending on local time. In Figure 11 we observe largest increases from the initial value to the peak at $\Delta t = 3$h in the prenoon sector, 0900–1200 LT (15 mA/m), about half of that value in the morning, 0600–0900 LT and afternoon, 1200–1500 LT and the smallest effect in the evening. This local-time dependent gain in CEJ amplitude compares well with the magnetic activity dependent amplitude variations over a day as shown in Figure 4b. This observation is consistent with our inference that the magnetic activity-dependent amplifications of CEJs are primarily caused by the disturbance wind dynamo. It would be desirable to verify that statement by concurrent observations of wind and currents.

5. Summary

By utilizing 10 years of geomagnetic field observations by the CHAMP satellite, we have presented the first global and comprehensive investigation of the counter equatorial electrojet (CEJ). There are many processes that can cause the current in the electrojet to flow westward. CEJ events can be found on average in 18% of all reliable electrojet profiles on the dayside (0600–1800 LT). The typical amplitude of the CEJ is significantly smaller than that of the EEJ. About 90% of the events exhibit peak current densities of less than 60 mA/m, with a most probable value of about 20 mA/m. We have systematically checked the dependences of the CEJ events, parameterized by their amplitude, occurrence rate, and HMW, on several environmental conditions. Furthermore, the solar and lunar tidal characteristics of the CEJ occurrence rate are analyzed and discussed. Finally, the response of the CEJ to changes of solar wind input has been investigated in this study. The main findings are summarized below:

1. The CEJ events show a clear local time variation. It is found that the CEJ amplitudes are largest around noontime and smaller in the morning and evening sectors, which can be attributed to the increased ionospheric conductivity at midday. Conversely, the CEJ occurrence rate is minimal around noon, very large at early morning, and large in the evening. Due to the smaller EEJ amplitudes in the morning and evening sectors, it is easier for additional influences (e.g., local winds or additional E fields) to reserve the current direction.
2. The seasonal variation of the CEJ occurrence rate is prominent. We find a broader maximum around July–August and a secondary peak in rate during January. The summertime enhancement is well synchronized with the count rate of meteor trails. We therefore assume an influence of the CEJ occurrence by the dust layer from meteor ablation. The meteor-related effect is strongest in longitude sectors where the magnetic equator is located in the Northern Hemisphere. The occurrence peak in January we attribute to the enhanced modulation of the EEJ current density (including reversal of current direction) by lunar tides during years of stratospheric sudden warmings. These polar events in the Northern Hemisphere occur typically around January.
3. The level of magnetic activity is most important for the amplitude of CEJ events. We find a linear dependence of the CEJ amplitude on the value of prevailing a_P index. The peak current density rises on average by 1 mA/m when a_P increases by 2 nT. During strong magnetic storms, CEJ current density can exceed 160 mA/m. But even without magnetic activity an average baseline amplitude of about 20 mA/m is found. Other processes (mainly tides) are responsible for these westward currents at quiet time. Also, the CEJ occurrence rates increase with magnetic activity but not so much as the amplitude.
4. Generally, the probability for CEJ to occur is higher during low solar activity. The occurrence rate reduces by about a factor of 2 from solar minimum to solar maximum. Interestingly, there is almost no dependence found of the average CEJ amplitude on the level of solar activity.

5. The CEJ occurrence rate and amplitude exhibits prominent longitudinal patterns. These are mainly caused by nonmigrating solar tides. Most prominent during all seasons are WN1 patterns primarily related to the semidiurnal SW3, the stationary SPW1, and to some extent to the terdiurnal TW4 components. Around December solstice the SW4, related to WN2, is quite strong, and in June the WN3, related to the diurnal DE2, is important. The well-known WN4 maximizes, as expected, during the months around August, and it is caused by the DE3 (driven from below) and the SPW4 tidal components. All these wave features are known from the analysis of EEJ modulation. But the respective wave crests appear out of phase between EEJ and CEJ.

6. Also, the lunar tide, in particular the semidiurnal M2 tide, contributes to the occurrence of CEJs. The strongest modulation of the electrojet intensity is observed during the months around January, in particular during years of stratospheric sudden warming events. Lunar tidal amplitudes are reduced by a factor of 2 around summer months. During times of small EEJ amplitudes, in the morning and evening, the lunar tidal features of the CEJ are much more pronounced than around noontime. Also, in case of the lunar M2 tide the wave crests appear out of phase between EEJ and CEJ. Generally, atmospheric tidal winds are on average the most important driver for CEJ occurrence.

7. Sudden changes of solar wind input have a significant influence on the CEJ occurrence. In case of a sudden increase in input, the transient eastward pointing prompt penetration electric field reduces the probability of CEJ occurrence. But about 3 hr after the event the westward directed disturbance dynamo electric field dominates, which enhances the occurrence rate and amplitude of the CEJs. This amplification lasts typically for more than 6 hr. The effect of the disturbance dynamo on CEJ is local time dependent. During prenoon and noon hours it is most efficient.

In this study we have presented climatological properties of the CEJ. Things we could not address are the temporal and spatial evolution of CEJs during individual events. This would require simultaneous multi-point observations, as provided, for example, by the Swarm constellation. This could be a topic for a follow-up study.

References

Alken, P., & Maus, S. (2007). Spatio-temporal characterization of the equatorial electrojet from CHAMP, Ørsted, and SAC-C satellite magnetic measurements. *Journal of Geophysical Research*, *112*, A09305. https://doi.org/10.1029/2007JA012524

Alken, P., Maus, S., Chulliat, A., Vigneron, P., Sirol, O., & Hulot, G. (2015). Swarm equatorial electric field chain: First results. *Geophysical Research Letters*, *42*, 673–680. https://doi.org/10.1002/2014GL062658

Alken, P., Maus, S., Vigneron, P., Sirol, O., & Hulot, G. (2013). Swarm SCARF equatorial electric field inversion chain. *Earth, Planets and Space*, *65*, 11. https://doi.org/10.5047/eps.2013.09.008

Bartels, J., & Johnston, H. F. (1940). Geomagnetic tides in horizontal intensity at Huancayo—Part I, terrestrial magnetism and atmospheric electricity. *Journal of Geophysical Research*, *45*, 269–308. https://doi.org/10.1029/TE045i003p00269

Blanc, M., & Richmond, A. D. (1980). The ionospheric disturbance dynamo. *Journal of Geophysical Research*, *85*, 1669–1686. https://doi.org/10.1029/JA085iA04p01669

Chandrasekhar, N. P., Archana, R. K., Nagarajan, N., & Arora, K. (2017). Variability of equatorial counter electrojet signatures in the Indian region. *Journal of Geophysical Research: Space Physics*, *122*, 2185–2201. https://doi.org/10.1002/2016JA022904

Chau, J. L., Goncharenko, L. P., Fejer, B. G., & Liu, H.-L. (2012). Equatorial and low latitude ionospheric effects during sudden stratospheric warming events. *Space Science Reviews*, *168*(1–4), 385–417. https://doi.org/10.1007/s11214-011-9797-5

Chen, P. R., Luo, Y., & Ma, J. (1995). The QBO modulation of the occurrence of the counter electrojet. *Geophysical Research Letters*, *22*, 2717–2720. https://doi.org/10.1029/95GL02796

Cohen, Y., & Achache, J. (1990). New global vector magnetic anomaly maps derived from Magsat data. *Journal of Geophysical Research*, *95*, 10,783–10,800. https://doi.org/10.1029/JB095iB07p10783

England, S. L., Maus, S., Immel, T. J., & Mende, S. B. (2006). Longitudinal variation of the *E*-region electric fields caused by atmospheric tides. *Geophysical Research Letters*, *33*, L21105. https://doi.org/10.1029/2006GL027465

Fejer, B. G., Jensen, J. W., & Su, S.-Y. (2008). Quiet time equatorial *F* region vertical plasma drift model derived from ROCSAT-1 observations. *Journal of Geophysical Research*, *113*, A05304. https://doi.org/10.1029/2007JA012801

Fejer, B. G., & Scherliess, L. (1995). Time dependent response of equatorial ionospheric electric fields to magnetospheric disturbances. *Geophysical Research Letters*, *22*, 851–854. https://doi.org/10.1029/95GL00390

Forbes, J. M., & Lindzen, R. S. (1976). Atmospheric solar tides and their electromagnetic effects, II, The equatorial electrojet. *Journal of Atmospheric and Terrestrial Physics*, *38*(9-10), 911–920. https://doi.org/10.1016/0021-9169(76)90074-X

Gouin, P. (1962). Reversal of the magnetic daily variation at Addis Ababa. *Nature*, *193*(4821), 1145–1146. https://doi.org/10.1038/1931145a0

Gouin, P., & Mayaud, P. N. (1967). A propos de l'existence possible d'un contre electrojet aux latitudes magnetiques equatoriales. *Annales Geophysicae*, *23*, 41–47.

Hagan, M. E., & Forbes, J. M. (2002). Migrating and nonmigrating diurnal tides in the middle and upper atmosphere excited by tropospheric latent heat release. *Journal of Geophysical Research*, *107*(D24), 4754. https://doi.org/10.1029/2001JD001236

Hagan, M. E., & Roble, R. G. (2001). Modeling the diurnal tidal variability with the National Center for Atmospheric Research thermosphere-ionosphere-mesosphere-electrodynamics general circulation model. *Journal of Geophysical Research*, *106*, 24,869–24,882. https://doi.org/10.1029/2001JA000057

Haldoupis, C., Pancheva, D., Singer, W., Meek, C., & MacDougall, J. (2007). An explanation for the seasonal dependence of midlatitude sporadic E layers. *Journal of Geophysical Research*, *112*, A06315. https://doi.org/10.1029/2007JA012322

Huang, C.-M., Richmond, A. D., & Chen, M.-Q. (2005). Theoretical effects of geomagnetic activity on low-latitude ionospheric electric fields. *Journal of Geophysical Research*, *110*, A05312. https://doi.org/10.1029/2004JA010994

Hutton, R., & Oyinloye, J. O. (1970). The counterelectrojet in Nigeria. *Annales Geophysicae*, *26*, 921–926.

Kelley, M. C., Makela, J. J., Chau, J. L., & Nicolls, M. J. (2003). Penetration of the solar wind electric field into the magnetosphere/ionosphere system. *Geophysical Research Letters*, *30*(4), 1158. https://doi.org/10.1029/2002GL016321

Kikuchi, T., Lühr, H., Kitamura, T., Saka, O., & Schlegel, K. (1996). Direct penetration of the polar electric field to the equator during a DP 2 event as detected by the auroral and equatorial magnetometer chains and the EISCAT radar. *Journal of Geophysical Research*, *101*, 17,161–17,173. https://doi.org/10.1029/96JA01299

Kikuchi, T., Pinnock, M., Rodger, A., Lühr, H., Kitamura, T., Tachihara, H., et al. (2000). Global evolution of a substorm-associated DP 2 current system observed by SuperDARN and magnetometers. *Advances in Space Research*, *26*, 121–124.

Lühr, H., & Manoj, C. (2013). The complete spectrum of the equatorial electrojet related to solar tides: CHAMP observations. *Annales Geophysicae*, *31*(8), 1315–1331. https://doi.org/10.5194/angeo-31-1315-2013

Lühr, H., Maus, S., & Rother, M. (2004). The noon-time equatorial electrojet, its spatial features as determined by the CHAMP satellite. *Journal of Geophysical Research*, *109*, A01306. https://doi.org/10.1029/2002JA009656

Lühr, H., Rother, M., Häusler, K., Alken, P., & Maus, S. (2008). The influence of non-migrating tides on the longitudinal variation of the equatorial electrojet. *Journal of Geophysical Research*, *113*, A08313. https://doi.org/10.1029/2008JA013064

Lühr, H., Siddiqui, T. A., & Maus, S. (2012). Global characteristics of the lunar tidal modulation of the equatorial electrojet derived from CHAMP observations. *Annales Geophysicae*, *30*(3), 527–536. https://doi.org/10.5194/angeo-30-527-2012

Marriot, R. T., Richmond, A. D., & Venkateswaran, S. V. (1979). The quiet-time equatorial electrojet and counter electrojet. *Journal of Geomagnetism and Geoelectricity*, *31*(3), 311–340. https://doi.org/10.5636/jgg.31.311

Marriot, R. T., Schieldge, J. P., Venkateswaran, S. V., & Cain, J. C. (1973). The quiet-time equatorial counter-electrojet. paper presented at the Second General Scientific Assembly of IAGA, September.

Mayaud, P. N. (1977). The equatorial counter electrojet: A review of its geomagnetic aspects. *Journal of Atmospheric and Terrestrial Physics*, *39*(9-10), 1055–1070. https://doi.org/10.1016/0021-9169(77)90014-9

McCreadie, H. (2004). Classes of the equatorial electrojet. In C. Reigber, et al. (Eds.), *Earth observation with CHAMP: Results from three years in orbit* (pp. 401–406). Berlin: Springer.

Newell, P. T., Sotirelis, T., Liou, K., Meng, C.-I., & Rich, F. J. (2007). A nearly universal solar wind-magnetosphere coupling function inferred from 10 magnetospheric state variables. *Journal of Geophysical Research*, *112*, A01206. https://doi.org/10.1029/2006JA012015

Oberheide, J., Forbes, J. M., Häusler, K., Wu, Q., & Bruinsma, S. L. (2009). Tropospheric tides from 80 to 400 km: Propagation, interannual variability, and solar cycle effects. *Journal of Geophysical Research*, *114*, D00I05. https://doi.org/10.1029/2009JD012388

Onwumechili, C. A. (1997). *The equatorial electrojet*. The Netherlands: Gordon and Breach Science Publishers.

Pedatella, N. M., & Liu, H. (2013). The influence of atmospheric tide and planetary wave variability during sudden stratosphere warmings on the low latitude ionosphere. *Journal of Geophysical Research: Space Physics*, *118*, 5333–5347. https://doi.org/10.1002/jgra.50492

Raghavarao, R., & Anandarao, B. G. (1980). Vertical winds as a plausible cause for equatorial counter electrojet. *Geophysical Research Letters*, *7*, 357–360. https://doi.org/10.1029/GL007i005p00357

Rao, K. N., & Rajarao, K. S. (1963). Quiet day magnetic variations near the magnetic equator. *Nature*, *200*(4905), 460–461. https://doi.org/10.1038/200460a0

Rastogi, R. G. (1973). Counter equatorial electrojet currents in the Indian zone. *Planetary and Space Science*, *21*(8), 1355–1365. https://doi.org/10.1016/0032-0633(73)90228-6

Rastogi, R. G. (1974a). Westward equatorial electrojet during daytime hours. *Journal of Geophysical Research*, *79*, 1503–1512. https://doi.org/10.1029/JA079i010p01503

Rastogi, R. G. (1974b). Lunar effects in the counter electrojet near the magnetic equator. *Journal of Atmospheric and Terrestrial Physics*, *36*(1), 167–170. https://doi.org/10.1016/0021-9169(74)90074-9

Reigber, C., Lühr, H., & Schwintzer, P. (2002). CHAMP mission status. *Advances in Space Research*, *30*(2), 129–134. https://doi.org/10.1016/S0273-1177(02)00276-4

Richmond, A. D., Lathuillére, C., & Vennerstroem, S. (2003). Winds in the high-latitude lower thermosphere: Dependence on the interplanetary magnetic field. *Journal of Geophysical Research*, *108*(A2), 1066. https://doi.org/10.1029/2002JA009493

Sastri, N. S., & Arora, B. R. (1981). Lunar modulation on the occurrence frequency of the afternoon counter-electrojet events at Trivandrum. *Planetary and Space Science*, *29*(10), 1091–1094. https://doi.org/10.1016/0032-0633(81)90007-6

Siddiqui, T. A., Lühr, H., Stolle, C., & Park, J. (2015). Relation between stratospheric sudden warming and the lunar effect on the equatorial electrojet based on Huancayo recordings. *Annales Geophysicae*, *33*(2), 235–243. https://doi.org/10.5194/angeo-33-235-2015

Somayajulu, V. V., Cherian, L., Rajeev, K., Ramkumar, G., & Reddi, C. R. (1993). Mean wind and tidal components during counter electrojet events. *Geophysical Research Letters*, *20*, 1443–1446. https://doi.org/10.1029/93GL00088

Stening, R. J. (2011). Lunar tide in the equatorial electrojet in relation to stratospheric warmings. *Journal of Geophysical Research*, *116*, A12315. https://doi.org/10.1029/2011JA017047

Stening, R. J., Meek, C. E., & Manson, A. H. (1996). Upper atmospheric wind systems during reverse equatorial electrojet events. *Geophysical Research Letters*, *23*, 3243–3246. https://doi.org/10.1029/96GL02611

Stolle, C., Manoj, C., Lühr, H., Maus, S., & Alken, P. (2008). Estimating the daytime equatorial ionization anomaly strength from electric field proxies. *Journal of Geophysical Research*, *113*, A09310. https://doi.org/10.1029/2007JA012781

Tomás, A. T., Lühr, H., Rother, M., Manoj, C., Olsen, N., & Watari, S. (2008). What are the influences of solar eclipses on the equatorial electrojet? *Journal of Atmospheric and Solar - Terrestrial Physics*, *70*(11-12), 1497–1511. https://doi.org/10.1016/j.jastp.2008.05-009

Vichare, G., & Rajaram, R. (2011). Global features of quiet time counterelectrojet observed by Ørsted. *Journal of Geophysical Research*, *116*, A04306. https://doi.org/10.1029/2009JA015244

Vineeth, C., Mridula, N., Muralikrishna, P., Kumar, K. K., & Pant, T. K. (2016). First observational evidence for the connection between the meteoric activity and occurrence of equatorial counter electrojet. *Journal of Atmospheric and Terrestrial Physics*, *147*, 71–75. https://doi.org/10.1016/j.jastp.2016.07.007

Vineeth, C., Pant, T. K., Kumar, K. K., Jose, L., Sumod, S. G., & Alex, S. (2012). Counter equatorial electrojets: Analysis of the variability in daytime mesopause temperature and winds. *Journal of Atmospheric and Solar - Terrestrial Physics*, *75–76*, 115–121. https://doi.org/10.1016/j.jastp.2011.07.005

Vineeth, C., Pant, T. K., & Sridharan, R. (2009). Equatorial counter electrojets and polar stratospheric sudden warmings—A classical example of high latitude-low latitude coupling? *Annales Geophysicae*, *27*(8), 3147–3153. https://doi.org/10.5194/angeo-27-3147-2009

Xiong, C., Lühr, H., & Fejer, B. G. (2015). Global features of the disturbance winds during storm time deduced from CHAMP observations. *Journal of Geophysical Research: Space Physics*, *120*, 5137–5150. https://doi.org/10.1002/2015JA021302

Xiong, C., Lühr, H., & Fejer, B. G. (2016). The response of equatorial electrojet, vertical plasma drift and thermospheric zonal wind to enhanced solar wind input. *Journal of Geophysical Research: Space Physics*, *121*, 5653–5663. https://doi.org/10.1002/2015JA022133

Xiong, C., Lühr, H., & Stolle, C. (2014). Seasonal and latitudinal variations of the electron density nonmigrating tidal spectrum in the topside ionospheric *F* region as resolved from CHAMP observations. *Journal of Geophysical Research: Space Physics*, *119*, 10,416–10,425. https://doi.org/10.1002/2014JA020354

Yamazaki, Y. (2013). Large lunar tidal effects in the equatorial electrojet during northern winter and its relation to stratospheric sudden warming events. *Journal of Geophysical Research: Space Physics*, *118*, 7268–7271. https://doi.org/10.1002/2013JA019215

Zhou, Y.-L., Lühr, H., & Alken, P. (2018). The sidebands of the equatorial electrojet: General characteristic of the westward currents, as deduced from CHAMP. *Journal of Geophysical Research: Space Physics*, *123*, 1457–1476. https://doi.org/10.1002/2017JA024687

Zhou, Y.-L., Lühr, H., Alken, P., & Xiong, C. (2016). New perspectives on equatorial electrojet tidal characteristics derived from the Swarm constellation. *Journal of Geophysical Research: Space Physics*, *121*, 7226–7237. https://doi.org/10.1002/2016JA022713

Zhou, Y.-L., Lühr, H., Xiong, C., & Pfaff, R. F. (2016). Ionospheric storm effects and equatorial plasma irregularities during the 17–18 March 2015 event. *Journal of Geophysical Research: Space Physics*, *121*, 9146–9163. https://doi.org/10.1002/2016JA023122